AIMS Mathematics, 11(6): 15851–15886.
DOI: 10.3934/math.2026653
Received: 31 January 2026
Revised: 19 April 2026
Accepted: 30 April 2026
Published: 05 June 2026

https://www.aimspress.com/journal/Math

Research article

A unified procedure for the identification of reduced-order fractional models based on the process reaction curve

Juan J. Gude[1,*], Oscar Camacho[2], Antonio Di Teodoro[1] and Pablo García Bringas[1]

[1] University of Deusto, Faculty of Engineering, Avda. de las Universidades, 24, Bilbao 48007, Bizkaia, Spain

[2] Universidad San Francisco de Quito, Colegio de Ciencias e Ingenierias, Avenida Diego de Robles y Vía Interoceánica, Quito 170157, Ecuador

* **Correspondence:** Email: jgude@deusto.es; Tel: +349441390032817.

Abstract: This paper introduces a unified analytical method for the identification of fractional reduced-order models, specifically the fractional first-order plus dead time (FFOPDT) and fractional dual-pole plus dead time (FDPPDT) structures, using only three points from the open-loop step response. The method provides explicit parameter-estimation formulas that eliminate the need for iterative optimization, reducing computational effort while preserving the simplicity of traditional reaction-curve techniques. Numerical simulations demonstrate superior accuracy and robustness compared to existing analytical and hybrid techniques, especially for overdamped and S-shaped responses typical of thermal and chemical processes. The method is validated for fractional orders within the range $\alpha \in [0.5, 1.0]$, covering the most relevant dynamics observed in practice. Laboratory experiments on a thermal system confirm the model's applicability under real-world conditions, including measurement noise, limited sensor resolution, and hardware constraints. Because the workflow aligns with standard industrial identification practices and does not require specialized knowledge of fractional calculus, it provides a practical means to incorporate fractional-order modeling into proportional-integral-derivative (PID)-based process control.

Keywords: fractional-order systems; process identification; reduced-order models; reaction curve; fractional PID control
Mathematics Subject Classification: 26A33, 93B30, 93B40, 93C05, 93C15

1. Introduction

In industrial process control, the availability of simple yet reliable low-complexity mathematical representations plays a significant role in the synthesis and adjustment of model-based control

strategies, especially those relying on proportional-integral-derivative (PID)-based schemes [1]. Traditionally, this need has been met by integer-order approximations, with the first-order plus dead time (FOPDT) and second-order plus dead time (SOPDT) families becoming the industry standard [2]. These models have been widely adopted in industry and have effectively met this need across a broad range of applications. Nevertheless, despite their practical success, integer-order approximations often prove inadequate to accurately represent the dynamic behavior of real-world processes that exhibit memory effects, long dead times, or anomalous diffusion, phenomena frequently encountered in chemical, thermal, and electrical systems [3–5].

In recent decades, fractional calculus has emerged as a powerful mathematical framework for describing such phenomena, because fractional derivatives naturally capture the long-term memory and hereditary effects inherent in these systems. This capability has attracted increasing attention in fields as diverse as diffusion processes, viscoelasticity, electrical networks, and control systems [6]. More recently, the scope of the field has expanded even further, with researchers developing advanced computational approaches for noninteger differential equations and novel methodologies to tackle the identification of increasingly complex fractional-order systems [7, 8]. Driven by this growing interest, researchers have developed a variety of methodological approaches for system identification, tailoring each to specific application requirements. Whereas traditional classification often distinguishes between time-domain techniques and frequency-domain methods, modern strategies have increasingly moved toward numerical approximations. In particular, operational matrices based on Haar or Chebyshev polynomials, alongside data-driven metaheuristic algorithms and neural networks, now provide robust pathways for parameter optimization even when the underlying system structure is not fully known [9].

Motivated by these developments, fractional-order models have increasingly been adopted to overcome some of the limitations of classical integer-order representations [10]. By introducing non-integer-order derivatives, these models provide additional degrees of freedom and enable a more flexible description of systems whose dynamics lie between classical integer orders [5, 11]. Within this class of models, the fractional first-order plus dead time (FFOPDT) model has gained significant attention due to its favorable trade-off between mathematical simplicity and modeling accuracy. In this context, several analytical parameter identification methods based on the process reaction curve have been proposed in the literature. Representative contributions include graphical and numerical procedures [12], three-point analytical identification methods [13], and generalized frameworks that enhance flexibility by adapting to different reaction curve shapes [14, 15], including recent adaptations of classical techniques, such as Sundaresan's method, to identify fractional-order models [16].

Although the aforementioned analytical methods prioritize simplicity through the reaction curve, other numerical approaches have been developed to handle the mathematical complexity of fractional-order modeling. As previously noted, orthogonal-function-based techniques, specifically Haar wavelets and block pulse function (BPF) expansions, have been widely employed for the approximation of fractional differential equations and the identification of fractional-order systems. These approaches represent system signals using orthogonal bases and transform fractional operators into algebraic systems that can be efficiently solved numerically [17, 18]. For instance, Haar wavelet operational matrices have been successfully employed to transform fractional differential equations into algebraic systems for analysis, simulation, and parameter estimation purposes [19]. Similarly, block pulse function expansions have been used to construct operational matrices for fractional

integration and differentiation, enabling the numerical solution and parameter identification of fractional-order systems [20, 21]. Although these techniques can achieve high numerical accuracy and are particularly suitable for solving fractional differential equations, they typically require discretization of system dynamics and the manipulation of relatively large algebraic systems. This often increases computational complexity and reduces transparency compared to control-oriented analytical identification methods.

In contrast, reaction curve-based methods aim to preserve the simplicity of classical identification procedures standard in industrial practice. Their primary advantage is ability to derive reduced-order fractional models directly from experimental step-response data. By requiring minimal computational effort, these techniques are particularly suited for control engineering applications where simple and reproducible identification procedures are preferred.

Complementing these approaches, optimization-based techniques have also been explored for FFOPDT model identification, as they often yield improved accuracy at the expense of increased computational effort. For instance, [22] proposed a commande robuste d'ordre non entier (CRONE)-based approach, where the optimal parameters are determined by minimizing the absolute deviation between the predicted model output and the system step response. Similarly, [23] developed a time-domain method employing numerical fractional calculus, supporting both Mittag-Leffler and Grünwald-Letnikov definitions, combined with particle swarm optimization (PSO) to minimize the mean squared error (MSE). This line of research has been recently extended to edge computing applications to improve efficiency in resource-constrained environments [24]. Furthermore, although the integration of machine learning (ML) algorithms has gained traction, their direct deployment on industrial hardware like programmable logic controllers (PLCs) remains constrained by limited computational power and memory [25]. To address these limitations, a hybrid identification strategy was proposed in [26], in which the fractional order α is obtained via optimization, and K, T, and L are determined analytically, thereby achieving a balanced compromise between accuracy and computational efficiency.

Building upon these developments, recent attention has shifted toward the fractional dual-pole plus dead time (FDPPDT) model, which extends the classical dual-pole plus dead time (DPPDT) structure and is particularly well-suited for describing overdamped or S-shaped step responses commonly observed in industrial systems [27, 28]. When FFOPDT models fail to capture the underlying fractional dynamics, especially in high-order or composite fractional systems, the FDPPDT formulation enhances accuracy by representing the process dynamics through a dual-pole structure with noninteger differentiation. Notably, to the best of the authors' knowledge, the analytical identification procedure proposed in [27] remains the only systematic method specifically developed for FDPPDT models based on process reaction curves, effectively extending FFOPDT-based identification concepts to more complex fractional system responses.

From a practical perspective, accurate fractional reduced-order models are particularly important in control-oriented applications because the accuracy of the identified process model directly influences the achievable performance and robustness of PID-type controllers [29, 30] as well as those of more advanced control strategies [31, 32]. In this context, it is well-documented that plant operators and control engineers often face tight time constraints and therefore tend to rely on well-established, standardized identification procedures rather than on techniques that require extensive numerical optimization or specialized theoretical expertise [33]. Therefore, identification methodologies that

preserve the conceptual structure of classical reduced-order models are particularly advantageous in industrial practice.

Motivated by these practical considerations, the proposed fractional identification procedure follows a framework fully consistent with that commonly used for integer-order models, enabling practitioners to apply it without requiring specialized knowledge of fractional calculus. This compatibility with conventional industrial practices facilitates its adoption and mitigates the traditional reluctance toward the use of fractional-order models in industrial settings [33].

Despite these advances, several practical challenges remain. Many existing identification approaches rely on iterative optimization, numerical discretization techniques, or specialized fractional calculus tools, which often limit their adoption in industrial environments where simple and reproducible identification procedures are preferred. Furthermore, most analytical identification methods reported in the literature focus on a single fractional model structure, typically the FFOPDT model; meanwhile, systematic procedures capable of identifying both FFOPDT and FDPPDT structures within a unified framework remain largely unexplored. Consequently, there is a need for identification methodologies that retain the simplicity of classical reaction-curve techniques while extending their applicability to a broader range of fractional reduced-order models.

In this work, we propose a systematic analytical framework for the identification of fractional reduced-order models (FFOPDT and FDPPDT) using open-loop step-test data. Our approach integrates existing analytical relationships into a streamlined, implementation-oriented procedure that prioritizes simplicity and reproducibility without the need for complex optimization.

The key contributions of this study are summarized as follows:

(1) Unified identification framework: A unified procedure is developed for the identification of both FFOPDT and FDPPDT models, enabling a consistent treatment of reduced-order fractional systems regardless of whether they exhibit first-order or dominant double-pole dynamics.
(2) Three-point data-driven identification: The proposed method relies exclusively on three arbitrarily selected points from the process reaction curve, significantly reducing data requirements while maintaining consistency with standard industrial identification practices.
(3) Closed-form parameter estimation: The model parameters are obtained through an explicit analytical formulation, avoiding the need for iterative numerical optimization and simplifying practical implementation.
(4) Low-complexity and implementation-oriented approach: The method is computationally efficient and numerically robust, making it suitable for real-time applications and deployment on embedded control platforms.
(5) Comprehensive validation: The effectiveness of the proposed framework is demonstrated through both numerical benchmarking against representative identification methods and experimental validation on a laboratory-scale thermal process under realistic operating conditions.

The remainder of the paper is organized as follows. Section 2 provides the mathematical foundations supporting the proposed approach. Section 3 describes a unified analytical identification technique based on the reaction curve for fractional reduced-order models of both considered structures. Section 4 evaluates numerical simulation results assessing the accuracy of the method and its performance relative to benchmark approaches. Section 5 reports experimental validation using a

laboratory-scale thermal process prototype. Section 6 discusses the main practical aspects, industrial implications, and limitations of the proposed approach. Finally, Section 7 concludes the paper by summarizing the main results and outlining possible avenues for future research.

2. Mathematical background

This section presents the fundamental mathematical concepts and tools of fractional calculus necessary for the identification technique proposed in this work. It includes the Riemann-Liouville operators and their main properties along with polynomial-type functions and the Mittag-Leffler function, which are essential for fractional modeling. Furthermore, the solution of fractional differential equations using the Laplace transform is presented, analyzing its numerical implementation using the Grünwald-Letnikov approximation. Finally, the fractional-order models considered are introduced, specifically the FFOPDT and FDPPDT structures.

2.1. Fundamentals of fractional calculus

This subsection summarizes the essential concepts of fractional calculus required for the identification procedure, including the Riemann-Liouville fractional derivative and integral, their main properties, and illustrative examples.

Definition 2.1. *The Riemann-Liouville fractional integral of order $\alpha > 0$ is defined by (see [6, 34, 35]):*

$$\left(I_{a^+}^{\alpha} h\right)(x) = \frac{1}{\Gamma(\alpha)} \int_a^x \frac{h(t)}{(x-t)^{1-\alpha}}\, dt, \quad x > a. \tag{2.1}$$

We denote by $I_{a^+}^{\alpha}(L_1)$ the family of functions h representable as a fractional integral $I_{a^+}^{\alpha}\varphi$ with $\varphi \in L_1(a,b)$. Further details on the properties of this class can be found in [34, 35].

Definition 2.2. *Let $\left(D_{a^+}^{\alpha} h\right)(x)$ be the Riemann-Liouville fractional derivative of order $\alpha \in \mathbb{R}$, $0 < \alpha < 1$ (see [6, 34, 35]):*

$$\left(D_{a^+}^{\alpha} h\right)(x) = \frac{d}{dx} \frac{1}{\Gamma(1-\alpha)} \int_a^x \frac{h(t)}{(x-t)^{\alpha}}\, dt, \tag{2.2}$$

where $[\alpha]$ denotes the integer part of α, and Γ is the gamma function. Consequently, (2.2) can be written as $\left(D_t^{\alpha} f\right)(t) = d/dt\left(I_t^{1-\alpha} f\right)(t)$.

Theorem 2.1. *Consider a function where $h \in I_{a^+}^{\alpha}(L_1), \alpha > 0$ if and only if $I_{a^+}^{p-\alpha} h \in AC^p([a,b])$, $p = [\alpha] + 1$, and $(I_{a^+}^{p-\alpha} h)^{(k)}(a) = 0$, $k = 0, \ldots, p-1$.*

In this context, $AC^p([a,b])$ refers to the class of functions h that are $p-1$ times continuously differentiable, with their $(p-1)$-th derivative satisfying absolute continuity over the interval $[a,b]$. When this requirement is relaxed, this class can be extended to encompass functions admitting a summable fractional derivative. Moreover, as pointed out in [6, Section 2.3.6], the lack of the semigroup property in fractional derivatives motivates the following result:

Lemma 2.1. *Let $h \in AC^{p-1}([a,b])$, and assume that $h^{(p)} \in L_1(a,b)$. Under these conditions, the fractional differentiation operators satisfy the semigroup property $D_{a^+}^{\alpha}\left(D_{a^+}^{\gamma} h\right) = D_{a^+}^{\alpha+\gamma} h$ provided that the initial conditions $h^{(j)}(a^+) = 0$, $j = 0, 1, \ldots, p-1$, are fulfilled, with $p = [\gamma] + 1$. See [34, 35].*

Remark 2.1. *For the sake of analytical tractability and practical implementation, attention is restricted to the case* $\alpha \in (0,1)$. *Nevertheless, this line of reasoning can be readily generalized to arbitrary ranges of* α. *In addition, the fractional parameter* $\alpha_0 \in (0,1)$ *can likewise be incorporated into the Riemann-Liouville fractional derivative operator in Eq* (2.2), *as* $D_{+}^{\alpha} = D_{x_0}^{(1+\alpha_0)/2}$.

2.2. Necessary family of functions

It is worth noting that the Riemann-Liouville derivative of a constant is generally nonzero; nevertheless, it correctly reflects the behavior expected in the corresponding limiting case:

$$\lim_{\alpha\to 1}\left(D_{a^+}^{\alpha}1\right)(x) = \lim_{\alpha\to 1}\frac{(x-a)^{-\alpha}}{\Gamma(1-\alpha)} = 0. \tag{2.3}$$

The relationship between the Riemann-Liouville and Caputo derivatives is well-known and is not discussed here, as this work is restricted to the Riemann-Liouville formulation; see [6, 34, 35] for details. This subsection introduces a class of functions that extend the behavior of classical exponential and polynomial models and are essential for describing fractional-order systems. We present their one- and two-parameter formulations, outline their main analytical properties, and discuss how they arise naturally in fractional differentiation and integration. In addition, we examine the derivatives and integrals of functions exhibiting polynomial-like behavior, highlighting their relevance within this broader functional framework.

2.2.1. Polynomial function

Let $\mu, \alpha \in (0,1)$, $a > 0$, $\mathrm{k} \in \mathbb{N}$ and $\beta > -1$. Then:

Integral of a polynomial centered at a

$$I_a^{\alpha}\left[(t-a)^{\beta}\right] = \frac{\Gamma(\beta+1)}{\Gamma(\beta+\alpha+1)}(t-a)^{\beta+\alpha}.$$

Derivative of a polynomial centered at a

$$D_a^{\mu}\left[(t-a)^{\beta}\right] = \begin{cases} 0, & \beta = \mu - 1, \\ \frac{\Gamma(\beta+1)}{\Gamma(\beta-\mu+1)}(t-a)^{\beta-\mu}, & \text{otherwise.} \end{cases}$$

2.2.2. Mittag-Leffler function

The two-parameter Mittag-Leffler function, as presented in [35–37], is given for all $z \in \mathbb{C}$ by:

$$E_{\alpha,\beta}(z) = \sum_{r=0}^{\infty}\frac{z^r}{\Gamma(\alpha r+\beta)}, \quad \alpha > 0,\ \beta \in \mathbb{C}. \tag{2.4}$$

The one-parameter formulation is recovered by setting $\beta = 1$ and $E_{\alpha,1}(z) = E_{\alpha}(z)$, and the choice $\alpha = \beta = 1$ yields the classical exponential function $E_{1,1}(z) = e^z$. In this sense, the Mittag-Leffler function constitutes a natural extension of the exponential function [36, 37]. Several properties that are relevant for the present study are related to the fractional differentiation and integration of the Mittag-Leffler function. In particular, for $\alpha,\ \mu > 0, \beta \geq 0$, $a = 0$, and $\gamma \in \mathbb{C}$,

Derivative of a polynomial:

$$D_{0^+}^{\alpha}\left[t^{\mu-1}E_{\beta,\mu}(\gamma t^{\beta})\right] = t^{\mu-\alpha-1}E_{\beta,\alpha+\mu}(\gamma t^{\beta}). \tag{2.5}$$

Integral of a polynomial:

$$I_{0^+}^{\alpha}\left[t^{\mu-1}E_{\beta,\mu}(\gamma t^{\beta})\right](x) = t^{\mu+\alpha-1}E_{\beta,\mu-\alpha}(\gamma t^{\beta}). \tag{2.6}$$

Representative studies addressing the role of the Mittag-Leffler function in asymptotic stability and control theory are reported in [38, 39].

Remark 2.2. *It is important to emphasize that in classical fractional calculus, the usual differentiation rules such as the Leibniz rule or the chain rule do not hold in their standard form. Therefore, great care must be taken when computing the derivatives of complicated functions; see [40, 41].*

2.3. Fractional differential equations and the Laplace transform

This subsection presents the analytical framework for solving Riemann-Liouville fractional differential equations using the Laplace transform, providing explicit solution expressions suitable for the identification procedure proposed in this work.

Let D_{+}^{α} denote the Riemann-Liouville fractional derivative of order $\alpha > 0$, and assume that $f(t)$ is locally integrable on $(0, \infty)$ and of exponential order so that its Laplace transform exists.
The Laplace transform of the Riemann-Liouville derivative is given by

$$\mathcal{L}\{D_{+}^{\alpha}f(t)\} = s^{\alpha}F(s) - \sum_{k=0}^{n-1} s^{k}\left[D^{\alpha-k-1}f(t)\right]_{t=0^+}, \tag{2.7}$$

where $n-1 \leq \alpha < n$ and $F(s) = \mathcal{L}\{f(t)\}(s)$. The additional terms $\left[D^{\alpha-k-1}f(t)\right]_{t=0^+}$ represent the fractional initial conditions associated with the Riemann-Liouville operator [6, 42].

In many identification and control applications, the system is assumed to start from rest. Under this assumption, the fractional initial terms vanish:

$$\left[D_{+}^{\alpha-k-1}f(t)\right]_{t=0^+} = 0, \qquad k = 0, \ldots, n-1,$$

and the Laplace transform simplifies to

$$\mathcal{L}\{D_{+}^{\alpha}f(t)\} = s^{\alpha}\mathcal{L}\{f(t)\},$$

allowing the fractional derivative in the Laplace domain to be treated analogously to the classical integer-order case, where differentiation corresponds to multiplication by s.

To illustrate this framework, consider the fractional differential equation:

$$D_{+}^{2\alpha}y_{\alpha}(t) + D_{+}^{\alpha}y_{\alpha}(t) + y_{\alpha}(t) = t^{\alpha-1}K\,u(t-L), \tag{2.8}$$

where $u(\cdot)$ denotes the Heaviside step function, and K is a constant gain.

Taking Laplace transforms and assuming zero initial conditions yields

$$(s^{2\alpha} + s^{\alpha} + 1)Y(s) = K\,\mathcal{L}\{t^{\alpha-1}u(t-L)\}.$$

The solution in the time domain can be expressed using the Mittag-Leffler function:

$$E_\alpha(z) = \sum_{k=0}^{\infty} \frac{z^k}{\Gamma(\alpha k + 1)},$$

which generalizes the exponential function and plays a similar role in fractional-order differential equations. Consequently, the solution can be written as

$$y_\alpha(t) = C\, t^{\alpha-1} K\, u(t - L) + f(t) E_\alpha(t^\alpha), \tag{2.9}$$

where C is a constant determined by initial conditions, and $f(t)$ is a sufficiently regular function determined by the forcing term.

Remark 2.3. *Throughout this work, zero initial conditions are assumed, corresponding to a system starting from rest. In practice, this assumption is naturally satisfied when dynamics are expressed in terms of deviation variables with respect to a steady-state operating point. Under this assumption, the Laplace transform of the Riemann-Liouville derivative reduces to* $\mathcal{L}\{D^\alpha f(t)\} = s^\alpha F(s)$*, and the choice of initial conditions does not affect the parameter estimation framework.*

2.4. Numerical version

Based on the operator defined in (2.2), the Grünwald-Letnikov derivative is adopted as a discrete approximation of the Riemann-Liouville derivative for numerical implementation. In the limit, as the step size tends to zero, the Grünwald-Letnikov derivative converges to the continuous fractional derivative [6, 35]. In this work, the Grünwald-Letnikov derivative is preferred because its inherently discrete formulation makes it well-suited for numerical computation.

Definition 2.3. *Let* $\alpha > 0$*,* $f \in C^k[a, b]$*,* $k = \lceil \alpha \rceil$*, and* $a < x \leq b$*. Then,*

$$\begin{aligned} D_a^\alpha f(x) &= \lim_{N\to\infty} \frac{\Delta_{h_N}^\alpha f(x)}{h_N^\alpha} = \\ &= \lim_{h\to 0} \frac{1}{h^\alpha} \sum_{k=0}^{\infty} (-1)^k \binom{\alpha}{k} f(x - kh), = \\ \lim_{h\to 0} \frac{1}{h^\alpha} &\sum_{k=0}^{\infty} (-1)^k \binom{\alpha}{k} \frac{f(x - kh)}{\Gamma(n - \alpha)(x - kh - a)^{n-\alpha}} \end{aligned} \tag{2.10}$$

with $h = (x - a)/N$*,* $N = 1, 2, \ldots$*, and* $n - 1 < \alpha < n$*.*

2.5. Fractional-order process models

This subsection presents the fractional-order process models used throughout this study, namely the FFOPDT and FDPPDT formulations. These models generalize their integer-order counterparts by incorporating fractional derivatives, which allows a more faithful representation of processes with distributed dynamics or nonstandard transient behavior.

Both structures are particularly appropriate for describing overdamped processes with S-shaped responses. The FFOPDT model offers a compact representation of fractional first-order dynamics,

whereas the FDPPDT formulation introduces additional degrees of freedom, making it more suitable for systems whose transients display stronger curvature or effective higher-order effects.

The mathematical description of each model is given by

$$TD_{+}^{\alpha}y_{\alpha}(t) + y_{\alpha}(t) = Ku(t-L), \tag{2.11}$$

which characterizes first-order fractional dynamics. In contrast, the FDPPDT model is expressed as:

$$T^2D_{+}^{2\alpha}y_{\alpha}(t) + 2TD_{+}^{\alpha}y_{\alpha}(t) + y_{\alpha}(t) = Ku(t-L) \tag{2.12}$$

and is capable of capturing higher-order dynamics associated with more complex process responses. Here, D_{+}^{α} denotes the fractional derivative of order α, expressed using the Riemann-Liouville definition. In both models, $u(t)$ is the input signal, $y_{\alpha}(t)$ is the process output, K the gain, T the characteristic time constant, L the dead time, and α the fractional order, with $T > 0$ and $L \geq 0$.

Assuming zero initial conditions or using deviation variables, the transfer functions can be obtained as follows using the Laplace transform:

$$P(s) = \frac{Y_{\alpha}(s)}{U(s)} = \frac{\mathcal{L}\{y_{\alpha}(t)\}}{\mathcal{L}\{u(t)\}} = \frac{Ke^{-Ls}}{1+Ts^{\alpha}}, \tag{2.13}$$

$$P(s) = \frac{Y_{\alpha}(s)}{U(s)} = \frac{\mathcal{L}\{y_{\alpha}(t)\}}{\mathcal{L}\{u(t)\}} = \frac{Ke^{-Ls}}{(1+Ts^{\alpha})^2}. \tag{2.14}$$

Remark 2.4. *A detailed treatment of commensurability, along with its representation through polynomial-type rational functions, is presented in [26, 43].*

3. General analytical identification procedure

3.1. Unified approach for FFOPDT and FDPPDT models

A unified analytical identification method is introduced in this section for both FFOPDT and FDPPDT models based on open-loop step response data. The methodology builds on the approaches presented in [14] for FFOPDT models and [27] for FDPPDT models, and it provides a common identification framework applicable to both structures.

This work focuses on processes characterized by overdamped, S-shaped step responses. The proposed procedure effectively captures this behavior and enables the selection of either an FFOPDT or an FDPPDT model, depending on the desired trade-off between modeling accuracy and model complexity. Figure 1 illustrates a representative open-loop step response, providing the data required for model parameter identification.

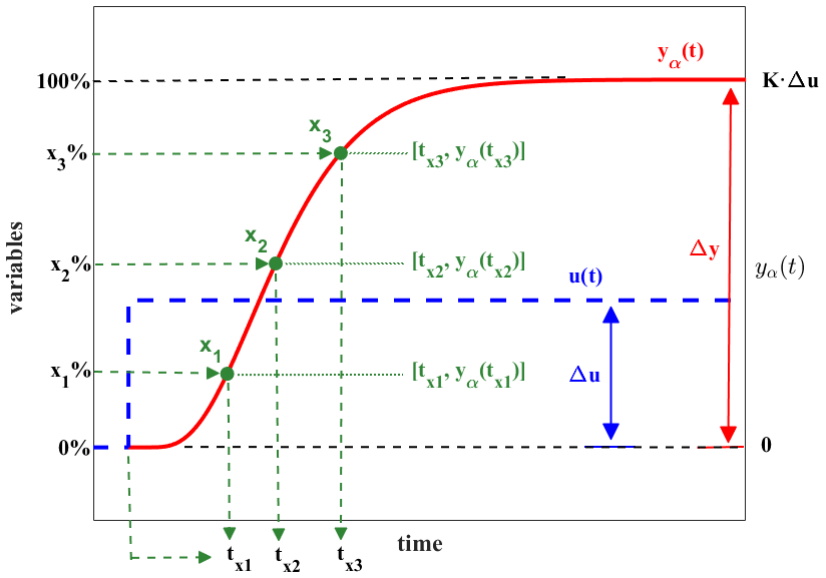

Figure 1. Open-loop step excitation and the corresponding process reaction curve $y_\alpha(t)$. The displayed response exhibits an overdamped fractional-order behavior, which can be accurately represented using FFOPDT or FDPPDT models. The figure also indicates the characteristic points of the response employed for parameter identification.

The time-domain responses to a step input of amplitude Δu for the FFOPDT model (2.13) and the FDPPDT model (2.14) are given by

$$y_\alpha(t) = K\Delta u \left\{1 - E_\alpha\left[-\frac{1}{T}(t-L)^\alpha\right]\right\}, \tag{3.1}$$

$$y_\alpha(t) = K\Delta u \left\{1 - \left(1 + \frac{(t-L)^\alpha}{T}\right) E_\alpha\left[-\frac{1}{T}(t-L)^\alpha\right]\right\}, \tag{3.2}$$

where K, T, L, and α are the model parameters common to both FFOPDT and FDPPDT structures; $\Delta y = K \cdot \Delta u$ represents the steady-state variation of the output; and E_α denotes the one-parameter Mittag-Leffler function [6].

With $\alpha = 1$, Eq (3.1) simplifies to the conventional FOPDT model, and Eq (3.2) reduces to the classical DPPDT formulation.

By scaling the output with respect to Δy and defining the normalized time variable $\tau = (t-L)^\alpha/T$, the following expressions are obtained:

$$\tilde{y}_\alpha(\tau) = \frac{y_\alpha(\tau)}{\Delta y} = 1 - E_\alpha(-\tau), \tag{3.3}$$

$$\tilde{y}_\alpha(\tau) = \frac{y_\alpha(\tau)}{\Delta y} = 1 - (1+\tau)E_\alpha(-\tau), \tag{3.4}$$

with $\tilde{y}_\alpha(\tau)$ indicating the normalized step response for each model.

The identification technique relies on three characteristic points extracted from the reaction curve. Let t_{x_i}, with $i = 1, 2, 3$, denote the time instants at which the system output reaches $x_i\%$ of the total

change, where $x_i \in [0, 100]$. Similarly, let τ_{x_i} denote the corresponding values in the normalized time domain at which the normalized model output $\tilde{y}_\alpha(\tau_x)$ reaches the same levels. Thus, $\{t_{x_1}, t_{x_2}, t_{x_3}\}$ and $\{\tau_{x_1}, \tau_{x_2}, \tau_{x_3}\}$ correspond to identical fractional output levels. The values τ_{xi} are obtained from the normalized model response, whereas t_{xi} are directly measured from the process step response.

The model parameters are estimated as follows [14, 27]:

$$\begin{cases} K = \dfrac{\Delta y}{\Delta u}, \\ \alpha = f_1(\Delta), \\ T = f_2(\alpha) \cdot (t_{x_3} - t_{x_1})^{\alpha}, \\ L = \max\left[t_{x_3} - f_3(\alpha) \cdot T^{1/\alpha},\ 0\right]. \end{cases} \tag{3.5}$$

In this formulation, the quantities $\{\Delta y, \Delta u, t_{x_1}, t_{x_2}, t_{x_3}\}$ are extracted directly from the measured step response. Functions f_1, f_2, and f_3 are empirical approximations (e.g., rational, polynomial, or exponential functions) obtained from curve fitting applied to data sets constructed from $\{\Delta,\ \alpha\}$, $\{\alpha,\ a^\alpha\}$, and $\{\alpha,\ \tau_{x_3}^{1/\alpha}\}$, respectively, with $\alpha \in [0.5, 1.0]$. Here, $a = 1/(\tau_{x_3}^{1/\alpha} - \tau_{x_1}^{1/\alpha})$, and $\Delta = (\tau_{x_3}^{1/\alpha} - \tau_{x_1}^{1/\alpha})/(\tau_{x_2}^{1/\alpha} - \tau_{x_1}^{1/\alpha})$, which can also be expressed in terms of measured times as $\Delta = (t_{x_3} - t_{x_1})/(t_{x_2} - t_{x_1})$.

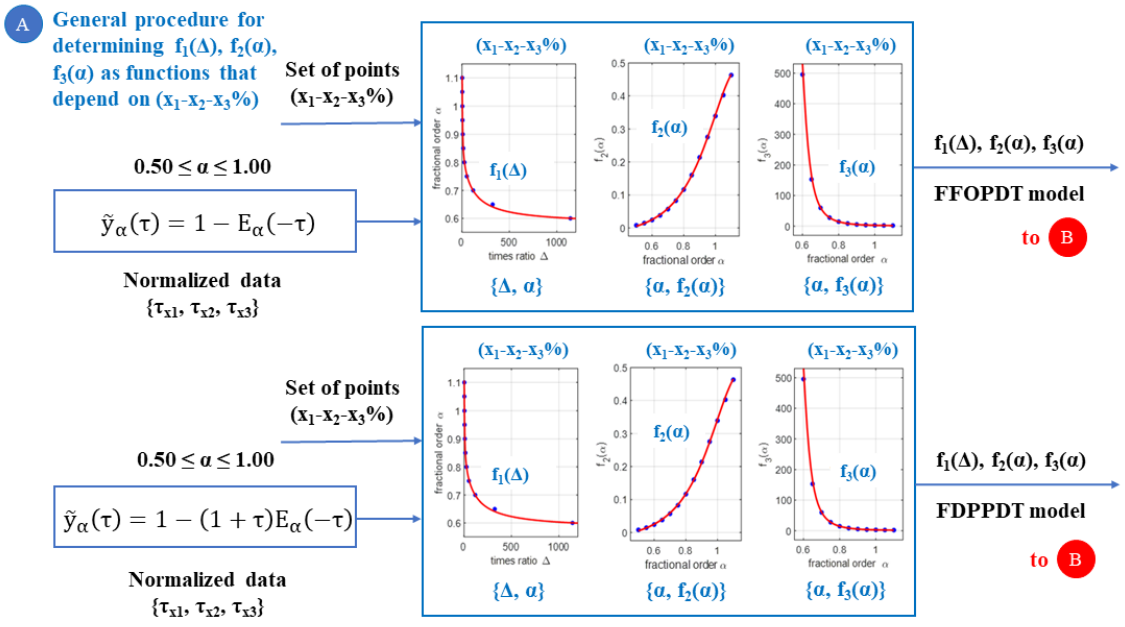

Figure 2. Stage A (offline) of the unified analytical identification methodology. This stage is devoted to constructing the auxiliary fitted functions $f_1(\Delta)$, $f_2(\alpha)$, and $f_3(\alpha)$ from the normalized step responses of the FFOPDT and FDPPDT models over the range $0.5 \leq \alpha \leq 1.0$.

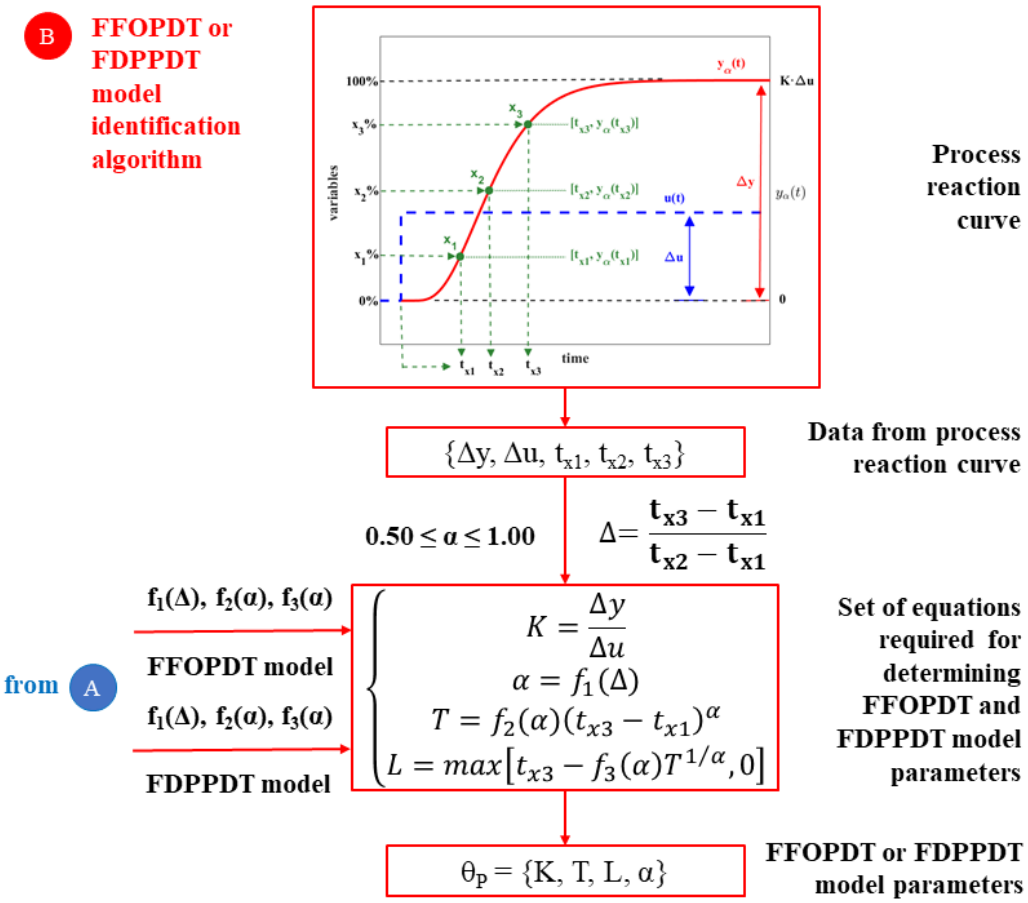

Figure 3. Stage B (online) of the unified analytical identification methodology. In this stage, the fitted auxiliary functions obtained in Stage A are combined with the measured data $\{\Delta y, \Delta u, t_{x_1}, t_{x_2}, t_{x_3}\}$, and a classical open-loop identification approach well-established in control engineering practice is applied to compute the parameters of the selected FFOPDT or FDPPDT fractional model using Eq (3.5).

Figures 2 and 3 illustrate a unified analytical identification methodology to estimate the parameters of fractional reduced-order models based on three selected points (x_1, x_2, x_3) extracted from the step response. The proposed methodology is structured into two complementary stages: Stage A (offline), where the auxiliary functions required by the identification process are constructed, and Stage B (online), where a classical open-loop identification approach, well-known to control engineers and plant technicians, is applied to compute the parameters of the selected fractional model.

Figure 2 summarizes the offline stage, during which the auxiliary functions f_1, f_2, and f_3 are derived. Their construction depends on several design choices:

(1) The selected model structure (FFOPDT or FDPPDT).
(2) The chosen set of points (x_1, x_2, x_3) on the reaction curve.
(3) The values of τ_{x_1}, τ_{x_2}, and τ_{x_3} over the range $0.5 \leq \alpha \leq 1.0$.
(4) The amount and quality of data, as well as the fitting strategy and the type and degree of the fitted functions.

These auxiliary functions are constructed from the normalized times $\{\tau_{x_1}, \tau_{x_2}, \tau_{x_3}\}$, obtained from the normalized step responses (3.3) and (3.4) for $0.50 \leq \alpha \leq 1.00$. Because this stage is carried out offline, the resulting fitted functions can be directly employed during the identification process through Eq (3.5).

Figure 3 illustrates the online stage of the proposed procedure, where the actual model identification is performed. In this stage, the auxiliary functions obtained offline are combined with the data set $\{\Delta y, \Delta u, t_{x_1}, t_{x_2}, t_{x_3}\}$. Using this information, the parameters of the selected fractional model (FFOPDT or FDPPDT) are computed following a classical open-loop identification approach that is well-established in industrial practice.

3.2. Choice of key points

The unified identification methodology applies to different selections of points (x_1-x_2-x_3%). Nevertheless, in the present study, the particular selection $x_1 = 10\%$, $x_2 = 65\%$, and $x_3 = 90\%$ is adopted. The proposed identification framework is not restricted to this particular configuration, and nearby values of the central point are expected to yield comparable performance.

An asymmetrical selection of characteristic points has been previously employed in this context; for instance, in [14] for the FFOPDT model and in [27] for the FDPPDT model. Specifically, this selection combines two previously reported findings: first, maintaining a wide separation between x_1 and x_3 [44], and second, moving the central point x_2 beyond 50% [45], both of which improve the accuracy of the identified model. Furthermore, this particular selection is supported by empirical observations and the authors' prior experience in applying various identification techniques for fractional models based on the reaction curve (see, e.g., [13, 14, 27, 39]).

Using these points, the data sets $\{\Delta,\ f_1(\Delta)\}$, $\{\alpha,\ f_2(\alpha)\}$, and $\{\alpha,\ f_3(\alpha)\}$ are generated from the normalized times $\{\tau_{10}, \tau_{65}, \tau_{90}\}$, with $0.50 \leq \alpha \leq 1.00$. The auxiliary functions f_1, f_2, and f_3 used to fit the experimental data are defined as follows:

$$f_k(x) = \frac{\sum_{i=0}^{n_k} p_{k,i} x^i}{\sum_{j=0}^{m_k} q_{k,j} x^j}, \tag{3.6}$$

where $k = 1, 2, 3$, and n_k and m_k are the orders of the numerator and denominator polynomials, respectively. The variable x represents Δ for $k = 1$ and α for $k = 2, 3$. The fitted coefficients $\{p_{k,i}, q_{k,j}\}$ for each function f_k were determined using Levenberg-Marquardt least-squares optimization based on the data described above. The resulting values for the FFOPDT and FDPPDT models are listed in Tables 1 and 2. The root mean square error (RMSE) reported for each fit confirms that the rational approximations faithfully reproduce the original data over the range $0.5 \leq \alpha \leq 1.0$, ensuring that the use of auxiliary functions adds no significant error to the identification process.

Table 1. Coefficients for the auxiliary functions f_k ($k = 1, 2, 3$) are used in the unified identification procedure for FFOPDT models, corresponding to the set (10–65–90%) selected on the step response.

$f_1(\Delta)$	$f_2(\alpha)$	$f_3(\alpha)$
$p_{1,1} = 0.3351$	$p_{2,1} = -0.0673$	$p_{3,1} = 4.066$
$p_{1,2} = 4.698$	$p_{2,2} = 0.1578$	$p_{3,2} = -7.705$
$p_{1,3} = -4.393$		$p_{3,3} = 5.055$
$q_{1,1} = 3.486$	$q_{2,1} = -2.501$	$q_{3,1} = -0.4136$
$q_{1,2} = -5.172$	$q_{2,2} = 1.699$	$q_{3,2} = 0.02868$
RMSE = $9.2 \cdot 10^{-4}$	RMSE = $1.8 \cdot 10^{-3}$	RMSE = $2.6 \cdot 10^{-3}$

Table 2. Coefficients for the auxiliary functions f_k ($k = 1, 2, 3$) used in the unified identification procedure for FDPPDT models, corresponding to the set (10–65–90%) selected on the step response.

$f_1(\Delta)$	$f_2(\alpha)$	$f_3(\alpha)$
$p_{1,1} = 0.3232$	$p_{2,1} = -0.0487$	$p_{3,1} = 6.79 \cdot 10^4$
$p_{1,2} = 3.8946$	$p_{2,2} = 0.0613$	$p_{3,2} = -1.40 \cdot 10^5$
$p_{1,3} = -5.7699$		$p_{3,3} = 8.70 \cdot 10^4$
$q_{1,1} = 2.0272$	$q_{2,1} = -2.2501$	$q_{3,1} = 8.93 \cdot 10^3$
$q_{1,2} = -4.7341$	$q_{2,2} = 1.2926$	$q_{3,2} = -6.01 \cdot 10^3$
		$q_{3,3} = 1.05 \cdot 10^3$
RMSE = $2.2 \cdot 10^{-4}$	RMSE = $6.5 \cdot 10^{-4}$	RMSE = $3.4 \cdot 10^{-2}$

Remark 3.1. *Although the unified methodology is designed for fractional-order models, it also encompasses the integer-order case when $\alpha = 1$. In this limit, the FFOPDT and FDPPDT structures reduce to the classical FOPDT and DPPDT models, respectively.*

The values of the auxiliary functions f_2 and f_3 are obtained by evaluating their fitted expressions at $\alpha = 1$, providing the parameters required for identifying integer-order models within the unified framework. The evaluation of f_1 is not required in this case, as it is used exclusively in the fractional formulation.

4. Simulation results

The following subsections present numerical case studies to assess the performance and versatility of the proposed unified three-point identification procedure. Section 4.1 examines a family of benchmark high-order fractional processes for evaluating the consistency of the method across a broad range of dynamic behaviors. Section 4.2 then focuses on a representative process from this family, comparing the FFOPDT and FDPPDT models obtained with the proposed approach against several existing fractional identification techniques. Finally, Section 4.3 evaluates the robustness of the proposed identification procedure by analyzing the sensitivity of the identified parameters to small variations in the characteristic points of the reaction curve.

4.1. Example 1

The following family of transfer functions is examined in this example:

$$P_{1,n}(s) = \frac{K_1}{(1 + T_1 s^{\lambda_1})^n} \tag{4.1}$$

with $K_1 = 2$, $T_1 = 1$ s, $\lambda_1 = 0.85$, and $n = 3, \ldots, 8$. This class of models represents high-order fractional processes dominated by repeated fractional poles and is inspired by the particular case $n = 5$ originally introduced in [12].

This example assesses the ability of the proposed unified identification procedure to accurately estimate both fractional reduced-order models across the family of benchmark processes.

Figure 4 illustrates the open-loop step responses corresponding to all processes defined in (4.1). The corresponding reaction curve data used for the identification of the considered fractional reduced-order models are summarized in Table 3. The parameters identified using the unified approach are reported for both fractional models in Tables 4 and 5, respectively, with $n = 3, \ldots, 8$.

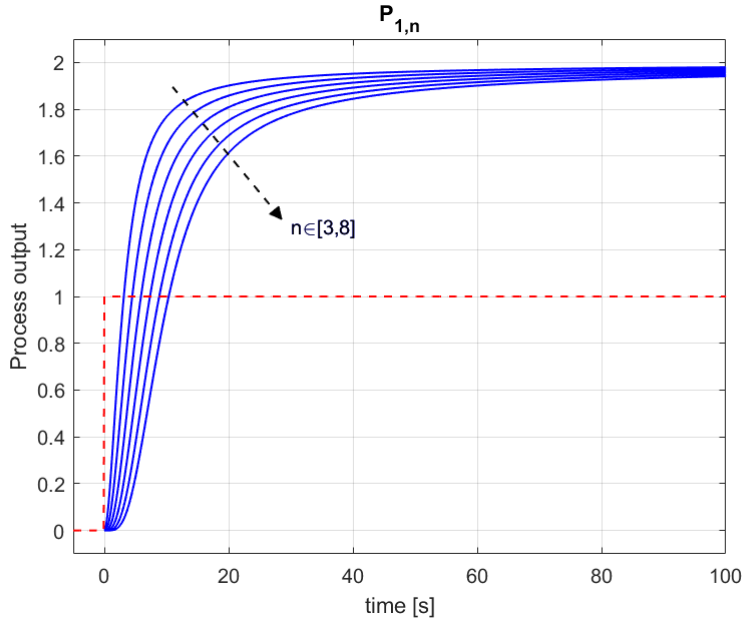

Figure 4. Step responses of the family of high-order fractional processes $P_{1,n}$ for $n \in [3, \ldots, 8]$ considered in the study. These responses illustrate the increasing system order and provide the benchmark processes used to evaluate the proposed identification method.

Table 3. Open-loop step response data for the family of processes $P_{1,n}$ ($n = 3, \ldots, 8$), used to identify FFOPDT and FDPPDT models through the proposed unified methodology.

n	Δu	Δy	t_{10}	t_{65}	t_{90}
3	1.00	2.00	0.97 s	4.34 s	11.08 s
4	1.00	2.00	1.62 s	6.05 s	15.06 s
5	1.00	2.00	2.35 s	7.81 s	19.20 s
6	1.00	2.00	3.13 s	9.62 s	23.42 s
7	1.00	2.00	3.97 s	11.43 s	25.55 s
8	1.00	2.00	4.84 s	13.38 s	33.10 s

Table 4. Parameters of the FFOPDT models identified from the family of processes $P_{1,n}$ ($n = 3, \ldots, 8$) using the proposed unified approach.

n	K	T	L	α
3	2.00	2.89 s	0.74 s	0.8902
4	2.00	3.66 s	1.33 s	0.8861
5	2.00	4.34 s	2.00 s	0.8800
6	2.00	5.00 s	2.73 s	0.8754
7	2.00	6.09 s	3.42 s	0.9037
8	2.00	6.02 s	4.36 s	0.8561

Table 5. Parameters of the FDPPDT models identified from the family of processes $P_{1,n}$ ($n = 3, \ldots, 8$) using the proposed unified approach.

n	K	T	L	α
3	2.00	1.41 s	0.32 s	0.8526
4	2.00	1.77 s	0.78 s	0.8494
5	2.00	2.09 s	1.33 s	0.8444
6	2.00	2.39 s	1.93 s	0.8407
7	2.00	2.88 s	2.47 s	0.8634
8	2.00	2.85 s	3.35 s	0.8246

The results reported in Tables 6 and 7 demonstrate the effectiveness of the proposed unified identification approach when applied to both considered model structures. Across the entire family of benchmark processes $P_{1,n}$, the FDPPDT structure consistently achieves lower MSE values than the FFOPDT, indicating its superior accuracy in capturing the dynamics of higher-order fractional processes dominated by repeated fractional poles. Nevertheless, FFOPDT models provide satisfactory approximations and are particularly advantageous when a reduced-order structure is required for control system design.

Table 6. MSE values $S(\theta_{1,n})$ for the FFOPDT models identified from the family $P_{1,n}$ ($n = 3, \ldots, 8$) using the proposed unified approach.

n	$S(\theta_{1,n})$
3	$1.16 \cdot 10^{-4}$
4	$1.76 \cdot 10^{-4}$
5	$2.25 \cdot 10^{-4}$
6	$2.82 \cdot 10^{-4}$
7	$6.23 \cdot 10^{-4}$
8	$3.42 \cdot 10^{-4}$
$N_S = 3\,001$	

Table 7. MSE values $S(\theta_{1,n})$ for the FDPPDT models identified from the family $P_{1,n}$ ($n = 3, \ldots, 8$) using the proposed unified approach.

n	$S(\theta_{1,n})$
3	$1.13 \cdot 10^{-5}$
4	$1.97 \cdot 10^{-5}$
5	$3.03 \cdot 10^{-5}$
6	$4.49 \cdot 10^{-5}$
7	$1.92 \cdot 10^{-4}$
8	$8.26 \cdot 10^{-5}$
$N_S = 3\,001$	

Overall, these results validate the unified approach as a reliable and consistent tool for estimating reduced-order fractional models and highlight its capability to guide the selection of the most appropriate model structure based on process characteristics and desired modeling accuracy.

Remark 4.1. *Because the identified models are obtained in explicit transfer-function form, their dynamic characteristics can also be analyzed in the frequency domain using standard tools such as Bode or Nyquist plots when required for controller design or robustness analysis. However, the proposed identification procedure is fundamentally based on time-domain reaction-curve data, which is consistent with standard industrial step-test identification practices.*

4.2. Example 2

In this second example, we focus on the process $P_{1,5}(s)$, which corresponds to the case $n = 5$ within the family introduced in Section 4.1. The remaining parameters are set to $K_1 = 2$, $T_1 = 1$ s, and $\lambda_1 = 0.85$. This model represents a high-order fractional process with repeated fractional poles, yielding a slow, monotonic step response and pronounced long-memory effects typical of fractional-order dynamics [6].

This example is intended to compare the accuracy of the FFOPDT and FDPPDT models estimated using the proposed unified method with that achieved by several existing techniques for identifying fractional-order reduced models. This allows us to assess the effectiveness of the unified three-point procedure for a representative process exhibiting dominant fractional dynamics.

From Table 3, the data associated with the case $n = 5$ are used to identify the proposed models for the process $P_{1,5}$. The corresponding identified parameters are reported in Tables 4 and 5.

Furthermore, the process $P_{1,5}$ was identified using several existing fractional reduced-order modeling techniques. Analytical methods based on symmetrical points were first considered, namely the FDPPDT approach of [27] and the FFOPDT method of [14], both applied to the (10–50–90%) set. Reaction-curve-based procedures employing asymmetrical points were also evaluated, including the method proposed by Nie in [13] for (20–60–95%). Additionally, the analysis considered the Mittag-Leffler-based FFOPDT method in [39] and the hybrid approach in [26], in which the fractional order α is obtained through single-variable optimization. The analytical procedures introduced in [12] were also included.

Figures 5 and 6 show the step responses of the FDPPDT and FFOPDT models identified using the unified procedure with the asymmetrical set (10–65–90%). For comparison, Figures 7 and 8 present the responses of the same models identified with the symmetrical set (10–50–90%). Additionally, Figures 9–12 depict the step responses of the models identified using the alternative identification approaches summarized in Table 8. Table 9 reports the MSE values obtained for all reduced-order models identified for the process $P_{1,5}$. The results clearly show that the proposed FDPPDT model provides the most accurate approximation of the reaction curve, achieving an MSE approximately one order of magnitude lower than that of the corresponding FFOPDT model identified using the same unified procedure. Overall, these results confirm the robustness and effectiveness of the unified identification framework, which enables systematic estimation and comparison of FFOPDT and FDPPDT models without prior knowledge of the most appropriate structure and preserving industrial applicability.

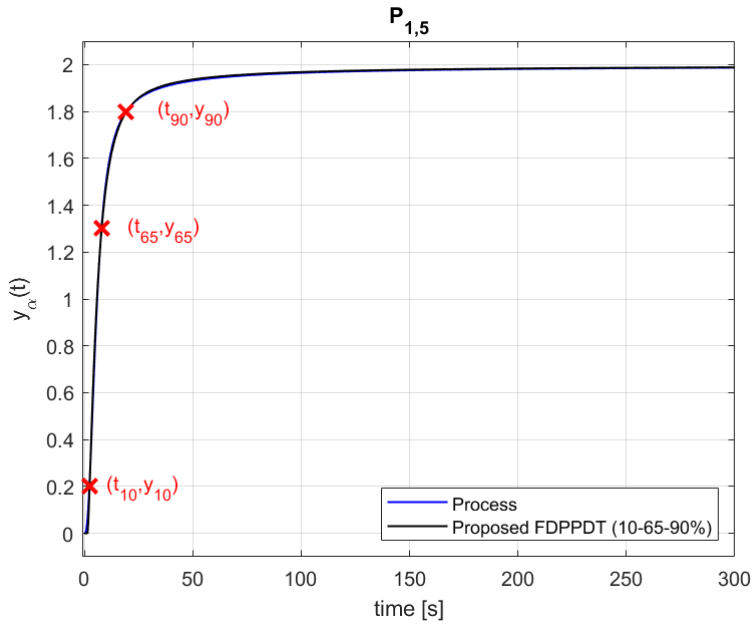

Figure 5. Step response of process $P_{1,5}$ and the FDPPDT model identified using the proposed unified three-point identification procedure with the set (10–65–90%). The figure shows the close agreement between the process and the reduced-order fractional model.

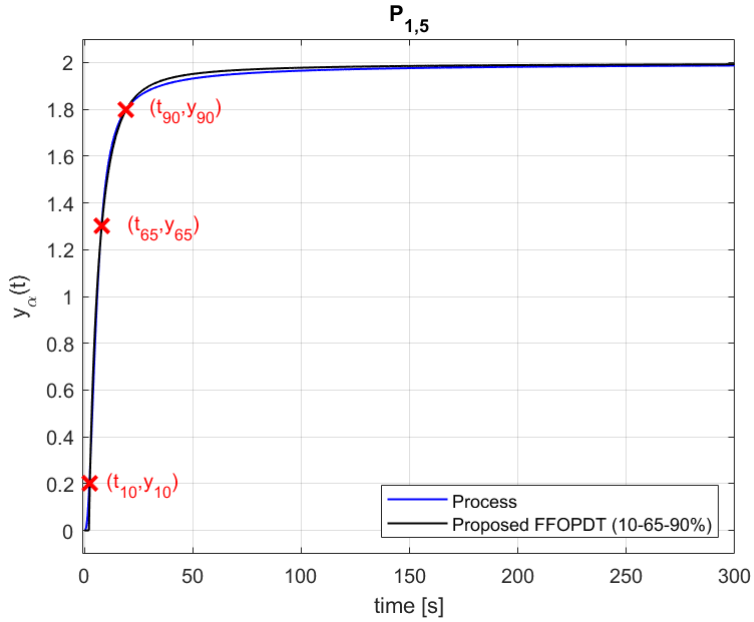

Figure 6. Step response of process $P_{1,5}$ and the FFOPDT model obtained using the proposed unified identification procedure with the set (10–65–90%). Compared with the FDPPDT model, larger deviations appear in the transient region.

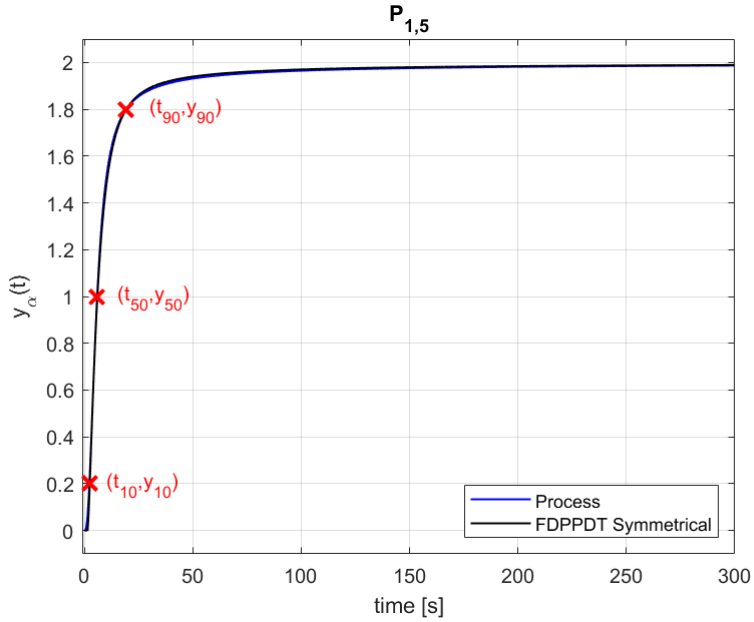

Figure 7. Comparison of the step response of process $P_{1,5}$ and the FDPPDT model identified using the symmetrical three-point identification approach in [27] for the set (10–50–90%), showing the agreement between the process dynamics and the reduced-order fractional model.

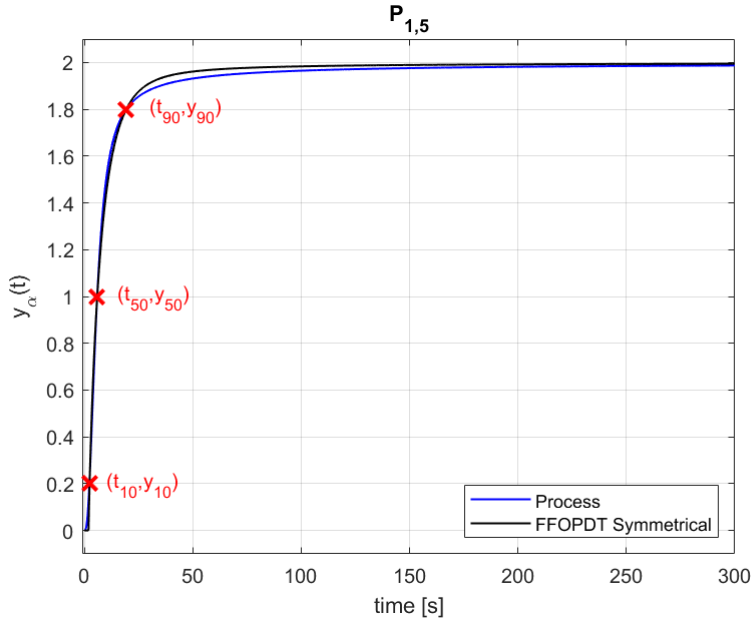

Figure 8. Comparison of the step response of process $P_{1,5}$ and the FFOPDT model identified using the symmetrical three-point identification approach in [14] for the set (10–50–90%), which provides accurate fitting at the selected identification points, although slight deviations may appear beyond the 90% region.

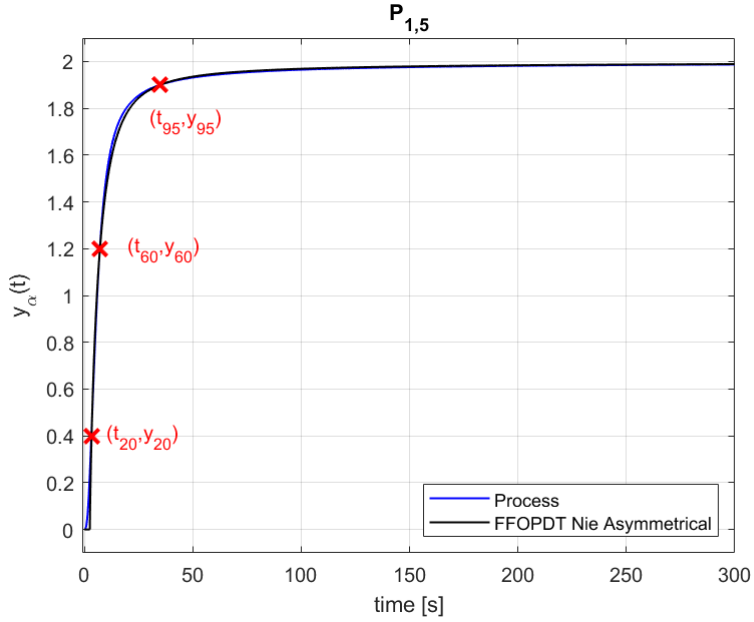

Figure 9. Comparison of the step response of process $P_{1,5}$ and the FFOPDT model identified using the asymmetrical three-point identification approach in [13] for the set (20–60–95%), illustrating the model approximation obtained with the asymmetrical fitting strategy.

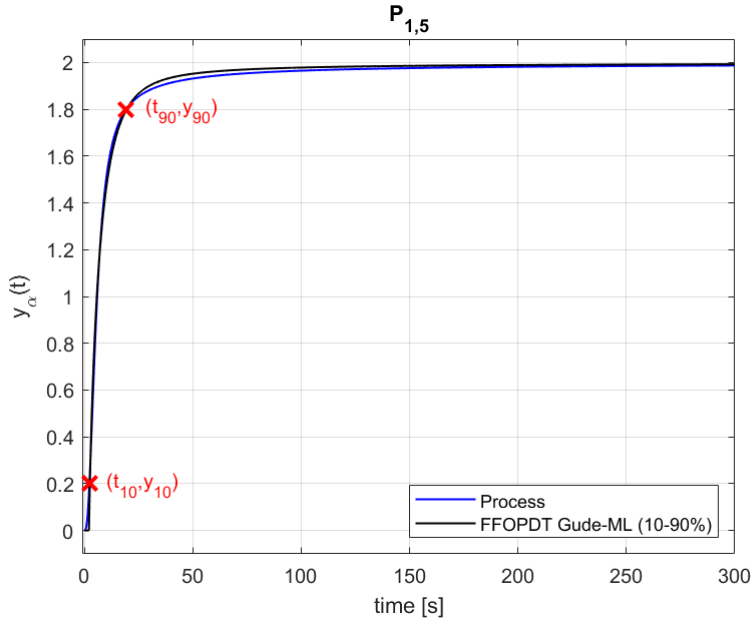

Figure 10. Comparison of the step response of process $P_{1,5}$ and the FFOPDT model identified using the method presented in [39], which exploits the asymptotic properties of the Mittag-Leffler function to estimate the fractional-order parameter α, using the set (10–90%).

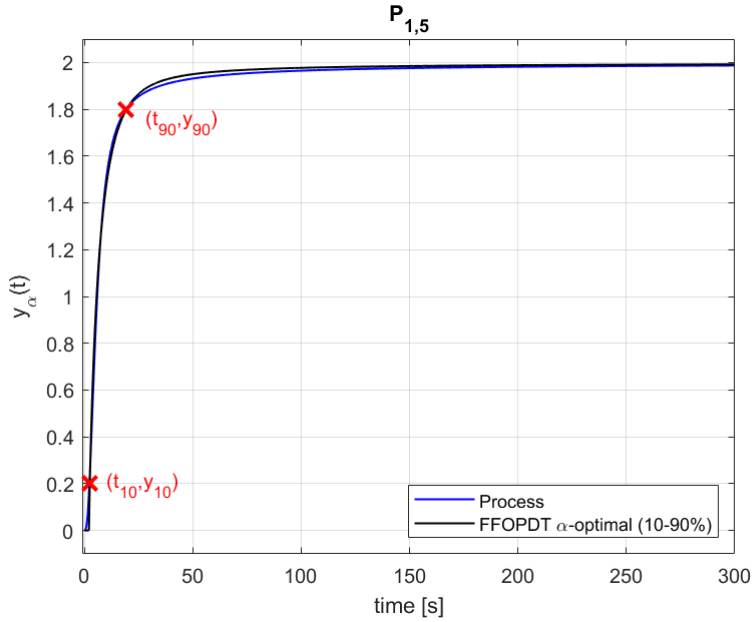

Figure 11. Step response of process $P_{1,5}$ and the FFOPDT model identified using the hybrid approach in [26] with the set (10–90%), which includes the optimization of the fractional-order parameter α. The resulting approximation still exhibits small deviations in the transient response.

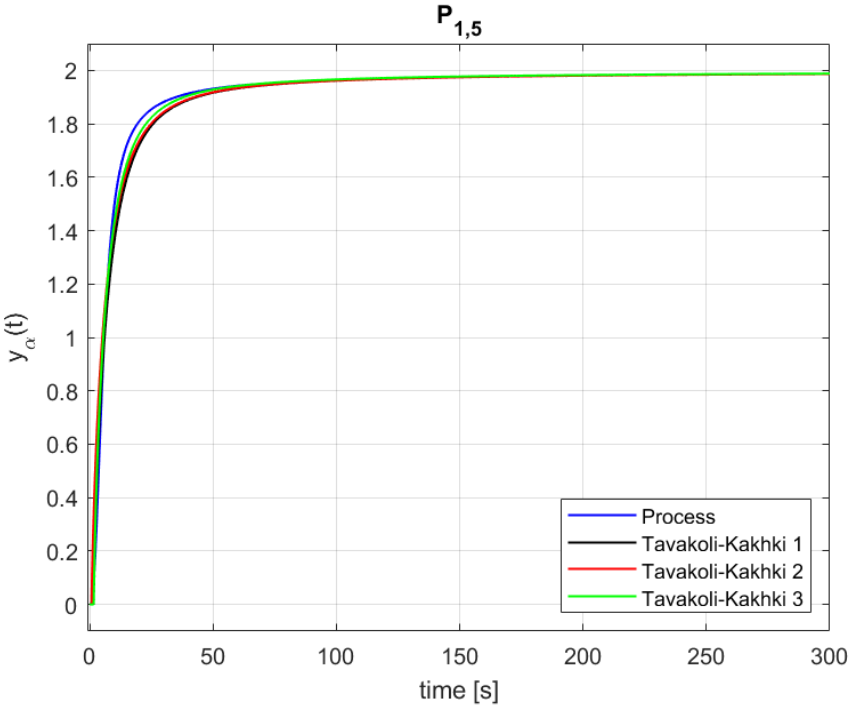

Figure 12. Step response of process $P_{1,5}$ and several FFOPDT models obtained using the identification methods reported in [12]. The figure provides a visual comparison of the different approximations and highlights the differences in transient-response accuracy.

Table 8. Fractional reduced-order model parameters for $P_{1,5}$ obtained using the various identification techniques ($j = 1, \ldots, 10$).

j	Method	Model	K	T	L	α
1	Proposed	FDPPDT	2.00	2.09 s	1.33 s	0.844
2	Proposed	FFOPDT	2.00	4.34 s	2.00 s	0.880
3	Symmetrical [27]	FDPPDT	2.00	2.20 s	1.39 s	0.855
4	Symmetrical [14]	FFOPDT	2.00	5.07 s	1.89 s	0.912
5	Nie asymmetrical [13]	FFOPDT	2.00	3.83 s	2.44 s	0.842
6	Gude Mittag-Leffler [39]	FFOPDT	2.00	4.44 s	2.00 s	0.884
7	Gude α-optimal [26]	FFOPDT	2.00	4.29 s	2.01 s	0.877
8	Tavakoli-Kakhki 1 [12]	FFOPDT	2.00	5.00 s	1.50 s	0.850
9	Tavakoli-Kakhki 2 [12]	FFOPDT	2.00	5.00 s	0.69 s	0.850
10	Tavakoli-Kakhki 3 [12]	FFOPDT	2.00	4.48 s	1.50 s	0.850

Table 9. Computed mean squared error values $S(\theta_{1,j})$ for the reduced-order models identified for $P_{1,5}$ with the various identification techniques ($j = 1, \ldots, 10$).

j	Method	Model	$S(\theta_{1,j})$
1	Proposed	FDPPDT	$2.98 \cdot 10^{-5}$
2	Proposed	FFOPDT	$2.45 \cdot 10^{-4}$
3	Symmetrical [27]	FDPPDT	$5.30 \cdot 10^{-5}$
4	Symmetrical [14]	FFOPDT	$3.81 \cdot 10^{-4}$
5	Nie asymmetrical [13]	FFOPDT	$2.10 \cdot 10^{-4}$
6	Gude Mittag-Leffler [39]	FFOPDT	$2.34 \cdot 10^{-4}$
7	Gude α-optimal [26]	FFOPDT	$2.18 \cdot 10^{-4}$
8	Tavakoli-Kakhki 1 [12]	FFOPDT	$9.30 \cdot 10^{-4}$
9	Tavakoli-Kakhki 2 [12]	FFOPDT	$1.50 \cdot 10^{-3}$
10	Tavakoli-Kakhki 3 [12]	FFOPDT	$4.65 \cdot 10^{-4}$
	$N_S = 3\,001$		

Remark 4.2. *It should be noted that the comparison presented in Tables 8 and 9 primarily focuses on analytical identification methods based on reaction-curve information. Although several identification procedures have been proposed in the literature for FFOPDT models, the FDPPDT structure has received comparatively little attention so far. Consequently, most of the available analytical methods correspond to the FFOPDT model structure. The hybrid approach in [26], which combines analytical parameter estimation with numerical optimization of the fractional-order parameter α, is included mainly to provide an additional reference point beyond purely analytical procedures.*

4.3. Sensitivity analysis

The robustness of the proposed identification procedure was evaluated by analyzing the sensitivity of the identified parameters to small perturbations in the characteristic points of the reaction curve, which may arise due to measurement noise.

Monte Carlo simulations were performed to assess this effect. In these experiments, random variations were introduced in the characteristic times t_{x_i} to emulate the effect of measurement noise according to

$$t_{x_i}^{(k)} = t_{x_i}(1 + \varepsilon_i^{(k)}), \tag{4.2}$$

where $\varepsilon_i^{(k)}$ is a zero-mean Gaussian random variable with a standard deviation corresponding to a predefined noise level. A similar perturbation was applied to the process gain K.

For each Monte Carlo realization, the identification procedure was applied using the perturbed values, and the resulting estimates of the parameters K, T, L, and α were recorded. This methodology quantitatively evaluates the robustness of the proposed unified method to small perturbations in the three characteristic points of the reaction curve caused by measurement noise.

A total of $N = 200$ simulations were performed for both the FFOPDT and FDPPDT models of process $P_{1,5}$. The distributions of the identified parameters were summarized in terms of mean values, standard deviations (Std. dev.), coefficients of variation (CV), and percentage deviations from the nominal values, as reported in Tables 10 and 11.

Table 10. Statistical results of the Monte Carlo sensitivity analysis for the FFOPDT model of process $P_{1,5}$, including nominal values, mean estimates, standard deviation, coefficient of variation, and percentage error for the identified parameters under perturbations of the characteristic points due to measurement noise.

Parameter	Nominal	Mean	Std. dev.	CV (%)	Error (%)
K	2.0000	1.9990	0.0394	1.9721%	−0.0504%
T	4.3400	4.4647	0.2503	5.6055%	2.8743%
L	2.0000	1.8840	0.0647	3.4322%	−5.8005%
α	0.8800	0.8845	0.0137	1.5456%	0.5167%
Noise level: 2%					

Table 11. Statistical results of the Monte Carlo sensitivity analysis for the FDPPDT model of process $P_{1,5}$, including nominal values, mean estimates, standard deviation, coefficient of variation, and percentage error for the identified parameters under perturbations of the characteristic points due to measurement noise.

Parameter	Nominal	Mean	Std. dev.	CV (%)	Error (%)
K	2.0000	1.9990	0.0394	1.9721%	−0.0504%
T	2.0900	2.1291	0.1142	5.3615%	1.8690%
L	1.3300	1.3213	0.0900	6.8152%	−0.6570%
α	0.8440	0.8480	0.0111	1.3070%	0.4729%
Noise level: 2%					

The results in Tables 10 and 11 show that the estimated parameters of the FFOPDT and FDPPDT models remain close to their nominal values, with low percentage errors, indicating that the method is inherently robust to small variations in the characteristic times. The coefficients of variation remain below 5% for most parameters, confirming a high level of robustness of the proposed method. Slightly higher variability is observed for the time constant T in the FFOPDT model (5.6%) and for T and L in the FDPPDT model (5.3% and 6.8%, respectively), suggesting a moderate sensitivity of these parameters to noise affecting the characteristic points of the reaction curve.

5. Experimental study

This section evaluates the practical application and implementation of the proposed unified identification procedure by deploying it on industrial hardware. To validate its performance, experiments have been conducted using a laboratory-scale thermal prototype.

5.1. Experimental setup

The experimental setup considered in this work consists of a laboratory-scale thermal prototype, the NI myRIO hardware platform, and a PC. The prototype, shown in Figure 13, is based on a longitudinal metallic element with a heat sink at one end. Three heating elements and four negative temperature coefficient (NTC) temperature sensors are evenly distributed along its length, allowing both the actuation and measurement of the temperature evolution in space and time. As illustrated in the figure, the thermal process depends on heat conduction through the metallic element, natural convection to the surrounding air and the heat sink, and forced convection induced by a fan. The metallic element is enclosed within a methacrylate duct, open at one end and fitted with a variable-speed fan at the other.

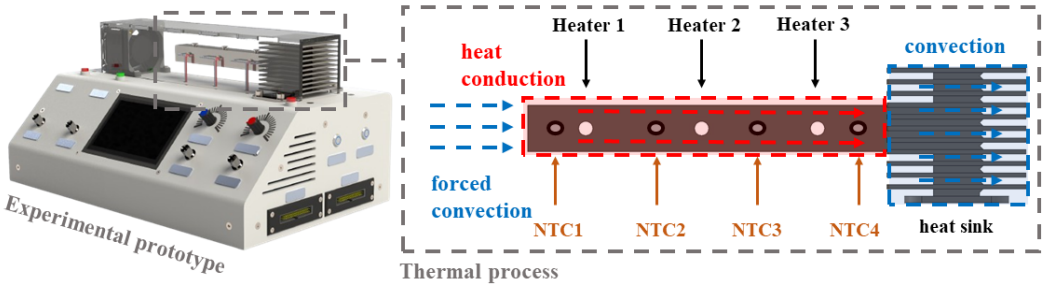

Figure 13. Experimental prototype including the area where the thermal process and its thermodynamic phenomena take place.

According to the block diagram shown in Figure 14, the thermal process has four input variables, namely the three command signals applied to the heating elements (u_{H1}, u_{H2}, and u_{H3}) and the fan signal (u_F). The outputs correspond to the temperatures measured by the four NTC sensors (T_{m1}, T_{m2}, T_{m3}, and T_{m4}).

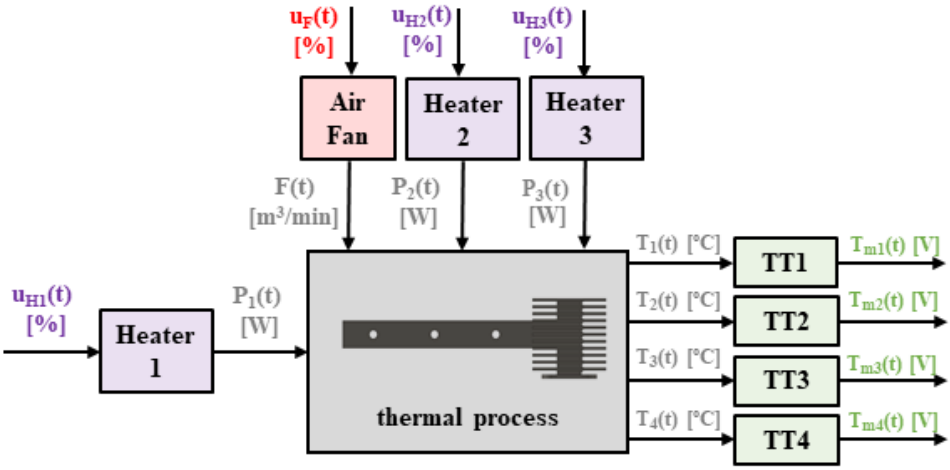

Figure 14. Block diagram of the thermal process with its components and variables.

5.2. Results and analysis

A step-test experiment is carried out following the steps below:

(1) A step change is applied to Heater 1, increasing its input from 30% to 50%.
(2) Heaters 2 and 3 are kept at 0%.
(3) The fan speed is set to 10%.
(4) The measured temperature T_{m2} is recorded, increasing from 39.75 to 52.77°C, corresponding to a temperature variation of $\Delta T_{m2} = 13.02$°C.

To reduce measurement noise, a low-pass digital filter is applied to the raw temperature signal prior to analysis. Such preprocessing strategies are commonly recommended in system identification and control applications (see, e.g., [46]). Specifically, a first-order low-pass filter was applied with a time constant $\tau_f = 1\ s$, which is well below the characteristic time scales of the process dynamics. This ensures effective attenuation of high-frequency measurement noise while preserving the shape of the reaction curve and avoiding distortion of the characteristic points used for identification.

The resulting reaction curve is then used to estimate the model parameters by applying the unified identification procedure with the suggested asymmetrical set (10–65–90%) and with the symmetrical set (10–50–90%), as commonly adopted in the literature (see, e.g., [27, 44]). The process data for both fractional models and both point selections are summarized in Table 12.

Table 12. Process measurements collected from the experimental response, employed for the estimation of the considered fractional-order models.

Process data information
$\Delta u = \Delta u_{H1} = 20\%$
$\Delta y = \Delta T_{m2} = 13.02\,^{\circ}\mathrm{C}$
$t_{10} = 50.40$ s
$t_{50} = 121.90$ s
$t_{65} = 155.30$ s
$t_{90} = 265.50$ s

Table 13 presents the identified model parameters obtained using the proposed unified identification framework. It includes the FDPPDT models identified with the asymmetrical set ($j = 1$) and the symmetrical set ($j = 2$) as well as the FFOPDT models estimated using the asymmetrical ($j = 3$) and symmetrical ($j = 4$) configurations.

Table 13. Estimated FDPPDT and FFOPDT model parameters for the thermal process, obtained via the unified identification procedure.

FDPPDT model parameters		
$\theta_{3,j}$	$j = 1$ ($x_2 = 65\%$)	$j = 2$ ($x_2 = 50\%$)
$K_{3,j}$	$K_{3,1} = 0.651°C/\%$	$K_{3,2} = 0.651°C/\%$
$T_{3,j}$	$T_{3,1} = 57.72$ s	$T_{3,2} = 58.55$ s
$L_{3,j}$	$L_{3,1} = 16.62$ s	$L_{3,2} = 22.24$ s
$\alpha_{3,j}$	$\alpha_{3,1} = 0.9856$	$\alpha_{3,2} = 0.9896$
FFOPDT model parameters		
$\theta_{3,j}$	$j = 3$ ($x_2 = 65\%$)	$j = 4$ ($x_2 = 50\%$)
$K_{3,j}$	$K_{3,3} = 0.651°C/\%$	$K_{3,4} = 0.651°C/\%$
$T_{3,j}$	$T_{3,3} = 166.50$ s	$T_{3,4} = 200.14$ s
$L_{3,j}$	$L_{3,3} = 34.90$ s	$L_{3,4} = 33.56$ s
$\alpha_{3,j}$	$\alpha_{3,3} = 1.0758$	$\alpha_{3,4} = 1.1034$

Figures 15 and 16 compare the measured temperature response of the thermal process with the responses of the FDPPDT models identified considering asymmetrical and symmetrical points, respectively. Similarly, Figures 17 and 18 present the corresponding comparisons for the FFOPDT models. These figures allow evaluating the ability of both model structures and point selections to reproduce the measured process dynamics.

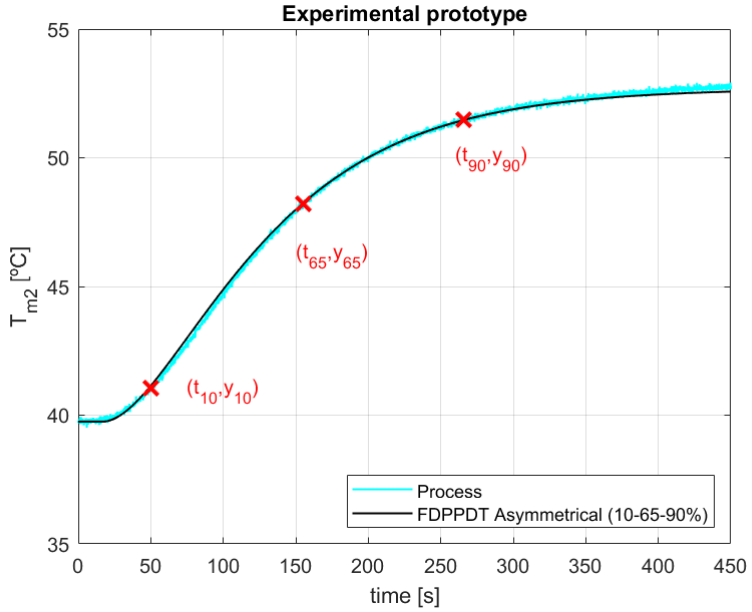

Figure 15. Comparison of the step response for the thermal prototype and that of the corresponding FDPPDT model identified using the unified procedure with the asymmetrical set (10–65–90%).

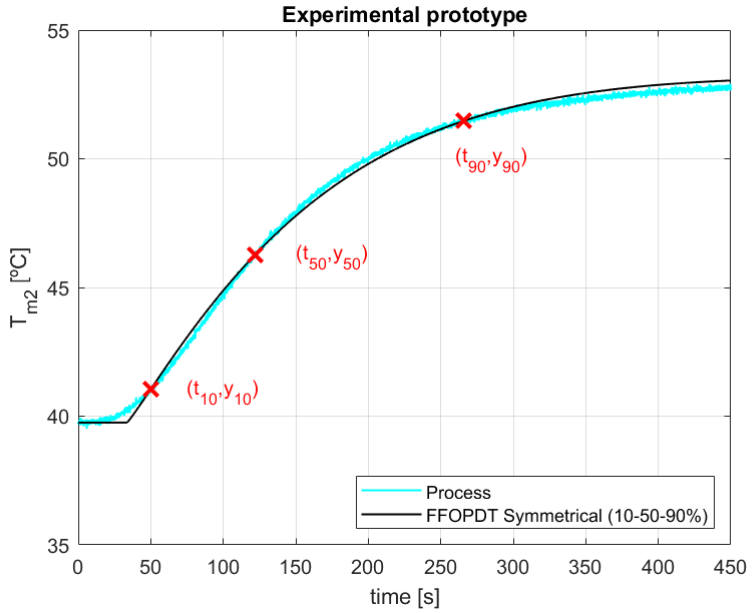

Figure 16. Comparison of the step response for the thermal prototype and that of the corresponding FDPPDT model identified using the unified procedure with the symmetrical set (10–50–90%).

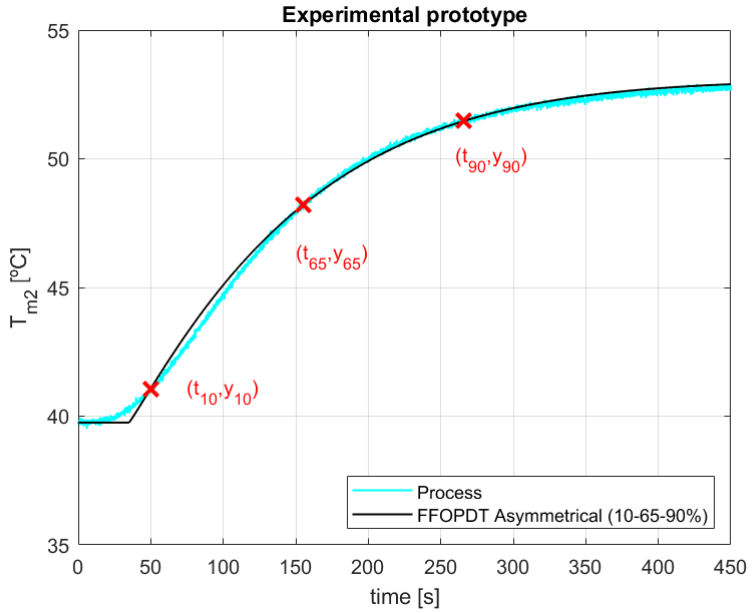

Figure 17. Comparison of the step response for the thermal prototype and that of the corresponding FFOPDT model identified using the unified procedure with the asymmetrical set (10–65–90%).

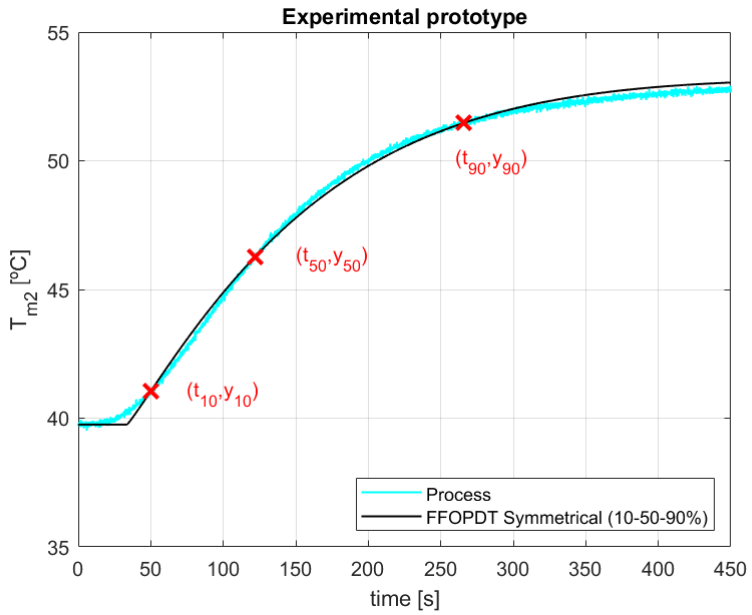

Figure 18. Comparison of the step response for the thermal prototype and that of the corresponding FFOPDT model identified using the unified procedure with the symmetrical set (10–50–90%).

Table 14 summarizes the accuracy of the identified models for the thermal process, quantified in terms of the MSE values $S(\theta_{3,j})$. The results clearly indicate that the FDPPDT structure outperforms the FFOPDT model for both point selections. In particular, the FDPPDT models (cases $j = 1$ and $j = 2$) exhibit approximately 50% lower MSE values than the FFOPDT models (cases $j = 3$ and $j = 4$). Moreover, the use of an asymmetrical set of identification points improves the accuracy of both model structures, confirming that this point selection provides a better representation of the process dynamics.

Table 14. Accuracy of the fractional reduced-order models for the thermal process, quantified by $S(\theta_{3,j})$ ($j = 1, \ldots, 4$), as determined using the unified approach.

j	Model	Set of points	$S(\theta_{3,j})$
1	FDPPDT	(10–65–90%)	$1.09 \cdot 10^{-2}$
2	FDPPDT	(10–50–90%)	$2.19 \cdot 10^{-2}$
3	FFOPDT	(10–65–90%)	$3.61 \cdot 10^{-2}$
4	FFOPDT	(10–50–90%)	$4.04 \cdot 10^{-2}$
		$N_S = 4\,501$	

Overall, these results demonstrate that the thermal process response is captured with higher accuracy when using the FDPPDT model, while preserving the same unified and low-complexity identification framework.

The identification procedure was implemented in LabVIEW using the microprocessor mode of the embedded platform described in [47], which is based on a dual-core 667 MHz ARM® Cortex™-A9 processor. This system operated with a sampling period of $T_S = 0.1$ s, and data acquisition yielded

N_S = 4500 samples. As the identification procedure only involves algebraic computations once the characteristic points are extracted, the computational burden is very low, and the identification can be performed in a fraction of a second, making it suitable for real-time or near real-time applications.

6. Discussion and industrial implications

In the previous sections, the applicability of the proposed unified identification technique has been demonstrated through simulation studies, as well as through implementation on industrial hardware and an experimental prototype. The results verify that a common approach can be established to estimate reduced-order fractional models using only the information provided by the process reaction curve.

The proposed method is examined below by considering several relevant elements, with particular emphasis on its practical implications and inherent constraints.

(1) Fractional-order structure

Within industrial practice, integer-order models, especially those of the FOPDT and DPPDT types, have become the conventional benchmark for PID controller tuning [1]. Their fractional-order extensions, FFOPDT and FDPPDT, are mathematically well-founded generalizations of their classical counterparts. By incorporating nonlocal dynamics, these models can more accurately reproduce the temporal responses of complex or higher-order systems.

Effective control system design often relies on accurate reduced-order fractional models. The unified procedure for identifying FFOPDT and FDPPDT models presented here represents an important step toward facilitating their adoption in industrial practice. To the best of author's knowledge, no analytical techniques currently allow the identification of both structures using a single methodology like the one proposed here.

(2) Trade-off between accuracy and computational complexity

Fractional-order models are widely recognized for capturing the dynamics of complex processes more accurately than integer-order models, particularly in overdamped or high-order responses. The FDPPDT structure, with its fractional double poles, is particularly suitable for higher-order processes, providing a more accurate step-response representation than FFOPDT models, while maintaining the same number of parameters and without increasing computational complexity.

From an analytical perspective, the identification procedure for both FDPPDT and FFOPDT models relies on closed-form expressions and shares the same parameter set $\{K, T, L, \alpha\}$, with only the auxiliary functions f_1, f_2, and f_3 differing between the two structures. Therefore, the method requires little computational effort and can be implemented on standard platforms, including PCs, PLCs, FPGAs, and microprocessor-based systems [47].

Consequently, the FDPPDT model provides higher accuracy with only a minor increase in computational effort. This makes it suitable for practical thermal applications, as shown in [27, 47, 48].

(3) Industry-oriented identification technique

The proposed identification method employs the standard open-loop step response test commonly used in industry [33]. The fractional-order parameters are obtained from explicit analytical formulas, eliminating the need for iterative optimization or specialized expertise in fractional calculus. Therefore, plant operators and control engineers can derive accurate models using procedures already familiar to them, making the method easier to apply in practice.

(4) Limitations and scope of applicability

The proposed identification procedure applies to processes with overdamped S-shaped step responses, which are common in systems governed by diffusion, heat transfer, or transport. Typical examples include thermal processes, electrochemical systems, distributed-parameter systems, and several chemical processes. The method is not suitable for systems with oscillatory or underdamped responses, which are more common in mechanical and electromechanical systems with dominant second-order dynamics and complex-conjugate poles. In these cases, model structures that explicitly account for oscillatory behavior are more appropriate.

In principle, the proposed identification framework is general and can be applied to fractional orders in the interval $0.00 < \alpha < 1.00$ (see [14,44]), corresponding to overdamped fractional-order dynamics. However, the auxiliary analytical expressions used in the procedure were derived for the interval $0.50 \leq \alpha \leq 1.00$, as many practical processes fall within this range. Consequently, the method was developed and tested primarily for this range. When the actual fractional order falls outside this interval, the analytical approximations may lose accuracy, so the estimated parameters should be used with care.

Finally, the proposed identification method relies on reaction-curve information obtained from step-response data. In practice, the measured signal may be affected by noise, filtering, and data acquisition limitations [49]. However, these effects are usually present in industrial measurements, where signal filtering is commonly applied. As a result, the filter behavior can be considered part of the overall process dynamics captured during identification. Therefore, the identified model reflects both the process and the measurement system, which is often the most useful representation for control purposes. Even with these practical limitations, the method remains as simple as classical reaction-curve approaches while extending them to fractional reduced-order models.

7. Conclusions

A unified analytical method was developed to identify the FFOPDT and FDPPDT fractional reduced-order models from only three points of the step response. The method retains the simplicity of classical reaction-curve techniques while extending them to processes with long delays, memory effects, or other fractional dynamics. Because the model parameters are obtained from explicit formulas, no iterative optimization is required, which simplifies the model's use in practical applications.

The simulation results showed that the proposed method is more accurate and robust than existing analytical and hybrid approaches, especially for overdamped and S-shaped responses. These processes represent the main class of systems considered in this work and usually involve fractional orders in the range $0.50 \leq \alpha \leq 1.00$. The experimental study carried out on a laboratory thermal process confirmed that the method also performs well under realistic conditions, including measurement noise and hardware limitations. In particular, the FDPPDT model provided a more accurate description of the process than the FFOPDT model. At the same time, the proposed framework allows the user to select the model that best balances accuracy and implementation complexity.

From an industrial perspective, the proposed method follows the same steps commonly used in practice. It does not require advanced knowledge of fractional calculus, which makes it easier to apply in environments where simplicity and reliability are important. In this way, the method offers a practical way to introduce fractional-order models into process control.

Future research will focus on developing automatic tuning rules for fractional-order PID controllers based on the identified models. In addition, adaptive or recursive extensions of the identification scheme will be investigated to enable real-time monitoring and control of processes with time-varying fractional dynamics in practical industrial applications. Further research will also address extending the proposed methodology to underdamped and integrating processes as well as the model's implementation on low-cost embedded hardware platforms.

Author contributions

Juan J. Gude: Writing—original draft, Writing—review & editing, Conceptualization, Methodology, Validation, Software, Supervision, Resources, Investigation. Oscar Camacho: Writing—review & editing, Methodology, Supervision, Funding acquisition, Investigation. Antonio Di Teodoro: Writing—original draft, Writing—review & editing, Methodology, Data curation, Investigation. Pablo García Bringas: Writing—review & editing, Funding acquisition, Project administration.

Use of Generative-AI tools declaration

During the preparation of this manuscript, the authors used DeepSeek R1 and Grammarly for English grammar correction and language refinement.

Acknowledgments

The authors acknowledge funding support from the Basque Government through the Research Group D4K-Deusto for Knowledge (IT1528 and IT1796-26). Universidad San Francisco de Quito also supported this work through the Poligrants Program under Grant 41983. This work was additionally supported by the Spanish Ministry of Science and Innovation through the projects QSERV (PID2021-124054OB-C33) and ATHENA-AEGIS (PID2024-155693NB-C43).

Conflict of interest

The authors declare that they have no conflicts of interest.

References

1. K. J. Åström, T. Hägglund, Advanced PID control, *IEEE Contr. Syst.*, **26** (2006), 98–101. https://doi.org/10.1109/MCS.2006.1580160
2. A. O'dwyer, *Handbook of PI and PID controller tuning rules*, World Scientific, 2009. https://doi.org/10.1142/p575
3. H. Sun, Y. Zhang, D. Baleanu, W. Chen, Y. Chen, A new collection of real world applications of fractional calculus in science and engineering, *Commun. Nonlinear Sci.*, **64** (2018), 213–231. https://doi.org/10.1016/j.cnsns.2018.04.019

4. I. Petráš, Volume 6 applications in control, In: *Handbook of fractional calculus with applications*, Boston: De Gruyter, 2019. https://doi.org/10.1515/9783110571745
5. C. A. Monje, Y. Chen, B. M. Vinagre, D. Xue, V. Feliu, *Fractional-order systems and controls: fundamentals and applications*, London: Springer, 2010. https://doi.org/10.1007/978-1-84996-335-0
6. I. Podlubny, *Fractional differential equations*, Academic Press, 1999.
7. L. Sadek, S. A. ldris, F. Jarad, The general caputo-katugampola fractional derivative and numerical approach for solving the fractional differential equations, *Alex. Eng. J.*, **121** (2025), 539–557. https://doi.org/10.1016/j.aej.2025.02.065
8. L. Sadek, A. Algefary, On quantum trigonometric fractional calculus, *Alex. Eng. J.*, **120** (2025), 371–377. https://doi.org/10.1016/j.aej.2025.02.005
9. K. Kothari, U. V. Mehta, R. Prasad, Fractional-order system modeling and its applications, *J. Eng. Sci. Technol. Rev.*, **12** (2019), 6. https://doi.org/10.25103/jestr.126.01
10. R. Almeida, N. R. Bastos, M. T. T. Monteiro, Modeling some real phenomena by fractional differential equations, *Math. Method. Appl. Sci.*, **39** (2016), 4846–4855. https://doi.org/10.1002/mma.3818
11. J. Sabatier, P. Lanusse, P. Melchior, A. Oustaloup, *Fractional order differentiation and robust control design: CRONE, H-infinity and motion control*, Springer, 2015. https://doi.org/10.1007/978-94-017-9807-5
12. M. Tavakoli-Kakhki, M. Haeri, M. S. Tavazoei, Simple fractional order model structures and their applications in control system design, *Eur. J. Control*, **16** (2010), 680–694. https://doi.org/10.3166/ejc.16.680-694
13. Z. Nie, Q. Wang, R. Liu, Y. Lan, Identification and pid control for a class of delay fractional-order systems, *IEEE/CAA J. Automatic.*, **3** (2016), 463–476. https://doi.org/10.1109/JAS.2016.7510103
14. J. J. Gude, P. García Bringas, Proposal of a general identification method for fractional-order processes based on the process reaction curve, *Fractal Fract.*, **6** (2022), 526. https://doi.org/10.3390/fractalfract6090526
15. J. J. Gude, F. B. Baraldi, I. Oleagordia, P. García Bringas, Analytical fractional reduced-order model identification method for processes with overdamped and underdamped response, *IFAC-PapersOnLine*, **58** (2024), 191–196. https://doi.org/10.1016/j.ifacol.2024.08.188
16. M. W. Campos, F. A. Ayres Jr, I. V. de Bessa, R. L. de Medeiros, P. R. Martins, E. kaminski Lenzi, et al., Fractional-order identification system based on sundaresan's technique, *Chaos Soliton. Fract.*, **185** (2024), 115132. https://doi.org/10.1016/j.chaos.2024.115132
17. A. Deb, A. Dasgupta, G. Sarkar, A new set of orthogonal functions and its application to the analysis of dynamic systems, *J. Franklin I.*, **343** (2006), 1–26. https://doi.org/10.1016/j.jfranklin.2005.06.005
18. S. K. Damarla, M. Kundu, A unified framework using orthogonal hybrid functions for solving linear and nonlinear fractional differential systems, *AppliedMath*, **5** (2025), 153. https://doi.org/10.3390/appliedmath5040153

19. Y. Li, W. Zhao, Haar wavelet operational matrix of fractional order integration and its applications in solving the fractional order differential equations, *Appl. Math. Comput.*, **216** (2010), 2276–2285. https://doi.org/10.1016/j.amc.2010.03.063

20. Y. Tang, H. Liu, W. Wang, Q. Lian, X. Guan, Parameter identification of fractional order systems using block pulse functions, *Signal Process.*, **107** (2015), 272–281. https://doi.org/10.1016/j.sigpro.2014.04.011

21. Y. Li, N. Sun, Numerical solution of fractional differential equations using the generalized block pulse operational matrix, *Comput. Math. Appl.*, **62** (2011), 1046–1054. https://doi.org/10.1016/j.camwa.2011.03.032

22. E. Guevara, H. Meneses, O. Arrieta, R. Vilanova, A. Visioli, F. Padula, Fractional order model identification: Computational optimization, In: *2015 IEEE 20th Conference on Emerging Technologies and Factory Automation (ETFA)*, 2015. https://doi.org/10.1109/ETFA.2015.7301630

23. B. B. Alagoz, A. Tepljakov, A. Ates, E. Petlenkov, C. Yeroglu, Time-domain identification of one noninteger order plus time delay models from step response measurements, *Int. J. Model. Simul. Sc.*, **10** (2019), 1941011. https://doi.org/10.1142/S1793962319410113

24. I. Fidalgo Astorquia, N. Gómez-Larrakoetxea, J. J. Gude, I. Pastor, Fractional-order system identification: Efficient reduced-order modeling with particle swarm optimization and ai-based algorithms for edge computing applications, *Mathematics*, **13** (2025), 1308. https://doi.org/10.3390/math13081308

25. D. Zamora-Arranz, P. Garcia-Bringas, J. J. Gude, J. Del Ser, Leveraging programmable logic controllers for machine learning applications in industrial setups, *Results Eng.*, 2026, 110194.

26. J. J. Gude, P. García Bringas, M. Herrera, L. Rincón, A. Di Teodoro, O. Camacho, Fractional-order model identification based on the process reaction curve: A unified framework for chemical processes, *Results Eng.*, **21** (2024), 101757. https://doi.org/10.1016/j.rineng.2024.101757

27. J. J. Gude, O. Camacho, A. Di Teodoro, P. García Bringas, Analytical method for the identification of higher-order fractional systems using fractional dual-pole plus dead-time models, *Results Eng.*, **26** (2025), 105574. https://doi.org/10.1016/j.rineng.2025.105574

28. V. M. Alfaro, R. Vilanova, Control of high-order processes: Repeated-pole plus dead-time models' identification, *Int. J. Control*, **97** (2024), 141–151. https://doi.org/10.1080/00207179.2021.1954240

29. H. Meneses, O. Arrieta, F. Padula, A. Visioli, R. Vilanova, Fopi/fopid tuning rule based on a fractional order model for the process, *Fractal Fract.*, **6** (2022), 478. https://doi.org/10.3390/fractalfract6090478

30. A. Di Teodoro, J. J. Gude, S. Vega, R. Chalco, R. Montaluisa, O. Camacho, Fractional-order hybrid 2-dof pid control with a complex basis: A novel framework for mimo systems, *Asian J. Control*, **28** (2026), 57–75. https://doi.org/10.1002/asjc.3781

31. A. Di Teodoro, M. Herrera, L. Rincon, J. J. Gude, O. Camacho, A hybrid control framework for chemical processes with long time delay: Theory and experiments, *ACS omega*, **9** (2024), 32469–32480. https://doi.org/10.1021/acsomega.3c10514

32. J. J. Gude, A. Di Teodoro, D. Agudelo, M. Herrera, L. Rincón, O. Camacho, Sliding mode control design using a generalized reduced-order fractional model for chemical processes, *Results Eng.*, **24** (2024), 103032. https://doi.org/10.1016/j.rineng.2024.103032

33. T. Hägglund, *Process control in practice*, Boston: De Gruyter, 2023. https://doi.org/10.1515/9783111104959

34. A. Kilbas, H. Srivastava, J. Trujillo, *Theory and applications of fractional differential equations*, elsevier, 2006.

35. S. Samko, A. Kilbas, O. Marichev, *Fractional integrals and derivatives: Theory and applications*, 1993.

36. S. Rogosin, The role of the mittag-leffler function in fractional modeling, *Mathematics*, **3** (2015), 368–381. https://doi.org/10.3390/math3020368

37. R. Gorenflo, A. A. Kilbas, F. Mainardi, S. V. Rogosin, *Mittag-Leffler functions, related topics and applications*, Berlin: Springer, 2020. https://doi.org/10.1007/978-3-662-61550-8

38. H. J. Haubold, A. M. Mathai, R. K. Saxena, Mittag-leffler functions and their applications, *J. Appl. Math.*, **3** (2015), 298628. https://doi.org/10.1155/2011/298628

39. J. J. Gude, A. Di Teodoro, O. Camacho, P. García Bringas, A new fractional reduced-order model-inspired system identification method for dynamical systems, *IEEE Access*, **11** (2023), 103214–103231. https://doi.org/10.1109/ACCESS.2023.3317230

40. J. Ceballos, N. Coloma, A. Di Teodoro, D. Ochoa-Tocachi, Generalized fractional cauchy-riemann operator associated with the fractional cauchy-riemann operator, *Adv. Appl. Clifford Algebras*, **30** (2020), 70. https://doi.org/10.1007/s00006-020-01096-2

41. N. Coloma, A. Di Teodoro, D. Ochoa-Tocachi, F. Ponce, Fractional elementary bicomplex functions in the riemann-liouville sense, *Adv. Appl. Clifford Algebras*, **31** (2021), 63. https://doi.org/10.1007/s00006-021-01165-0

42. K. Diethelm, N. J. Ford, Analysis of fractional differential equations, *J. Math. Anal. Appl.*, **265** (2002), 229–248. https://doi.org/10.1006/jmaa.2000.7194

43. H. Aboukheir, J. Romero, A. Di Teodoro, An approach for fractional commensurate order youla parametrization using q-weighted operator, In: *Proceedings of the 21st International Conference on Informatics in Control, Automation and Robotics (ICINCO 2024)*, 2024, 706–713. https://doi.org/10.5220/0013058700003822

44. J. J. Gude, P. García Bringas, Influence of the selection of reaction curve's representative points on the accuracy of the identified fractional-order model, *J. Math.*, **265** (2002), 7185131. https://doi.org/10.1155/2022/7185131

45. J. J. Gude, P. García Bringas, Improving a reaction curve-based analytical identification technique for fractional models, *Int. J. Dynam. Control*, **13** (2025), 106. https://doi.org/10.1007/s40435-025-01604-x

46. V. Romero Segovia, T. Hägglund, K. J. Åström, Measurement noise filtering for pid controllers, *J. Process Contr.*, **24** (2014), 299–313. https://doi.org/10.1016/j.jprocont.2014.01.017

47. J. J. Gude, P. García Bringas, A novel control hardware architecture for implementation of fractional-order identification and control algorithms applied to a temperature prototype, *Mathematics*, **11** (2023), 143. https://doi.org/10.3390/math11010143

48. K. Oprzedkiewicz, W. Mitkowski, E. Gawin, Application of fractional order transfer functions to modeling of high-order systems, In: *2015 20th International Conference on Methods and Models in Automation and Robotics (MMAR)*, 2015, 1169–1174. https://doi.org/10.1109/MMAR.2015.7284044

49. T. Hägglund, Signal filtering in pid control, *IFAC Proceedings Volumes*, **45** (2012), 1–10, 2012. https://doi.org/10.3182/20120328-3-IT-3014.00002

AIMS Press